The UBXN-2/p37/p47 adaptors of CDC-48/p97 regulate mitosis by limiting the centrosomal recruitment of Aurora A

Elsa Kress,[1,2] Françoise Schwager,[1,2] René Holtackers,[3] Jonas Seiler,[4] François Prodon,[1] Esther Zanin,[5] Annika Eiteneuer,[4] Mika Toya,[6] Asako Sugimoto,[7] Hemmo Meyer,[4] Patrick Meraldi,[1,3] and Monica Gotta[1]

[1]Department of Physiology and Metabolism, Faculty of Medicine, University of Geneva, 1211 Geneva, Switzerland
[2]Swiss National Centre for Competence in Research Program Chemical Biology, 1211 Geneva, Switzerland
[3]Institute of Biochemistry, ETH Zurich, CH-8093 Zurich, Switzerland
[4]Center for Medical Biotechnology, Faculty of Biology, Universität Duisburg-Essen, 45117 Essen, Germany
[5]Department of Cellular and Molecular Medicine, Ludwig Institute for Cancer Research, University of California, San Diego, La Jolla, CA 92093
[6]Laboratory for Cell Adhesion and Tissue Patterning, RIKEN Center for Developmental Biology, 650-0047 Kobe, Japan
[7]Laboratory of Developmental Dynamics, Tohoku University, 980-8577 Sendai, Japan

Coordination of cell cycle events in space and time is crucial to achieve a successful cell division. Here, we demonstrate that UBXN-2, a substrate adaptor of the AAA ATPase Cdc48/p97, is required to coordinate centrosome maturation timing with mitosis. In UBXN-2–depleted *Caenorhabditis elegans* embryos, centrosomes recruited more AIR-1 (Aurora A), matured precociously, and alignment of the mitotic spindle with the axis of polarity was impaired. UBXN-2 and CDC-48 coimmunoprecipitated with AIR-1 and the spindle alignment defect was partially rescued by co-depleting AIR-1, indicating that UBXN-2 controls these processes via AIR-1. Similarly, depletion in human cells of the UBXN-2 orthologues p37/p47 resulted in an accumulation of Aurora A at centrosomes and a delay in centrosome separation. The latter defect was also rescued by inhibiting Aurora A. We therefore postulate that the role of this adaptor in cell cycle regulation is conserved.

Introduction

Successful achievement of cell division requires tight temporal regulation of mitotic events (Tyson and Novak, 2008) and spatial coordination of the cleavage plane with the axis of chromosome segregation (Morin and Bellaïche, 2011). Impairing the mechanisms regulating such spatiotemporal coordination leads to major defects, which can be at the origin of pathologies like cancers and degenerative diseases. In asymmetrically dividing cells or in tissues, the cell division machinery must also be coordinated with the polarity axis or with the axis of the tissue. This is achieved by properly orienting the mitotic spindle (Morin and Bellaïche, 2011). Therefore, spatiotemporal coordination of cell division events is important not only at the cell level but also for the whole organism. One way to achieve such coordination is to regulate the localization and/or the degradation of key factors.

The conserved AAA ATPase Cdc48/p97 is a ubiquitously expressed protein first identified in yeast as a cell division cycle mutant gene (Fröhlich et al., 1991). Cdc48/p97 applies the energy of ATP hydrolysis to segregate protein complexes or extract proteins from subcellular structures (Meyer et al., 2012). In many cases, this involves ubiquitinated substrates and subsequently either degradation or recycling (Ye, 2006). This function confers to Cdc48/p97 various roles in regulating cellular processes, including cell division processes (Cao et al., 2003; Meyer and Popp, 2008; Cheng and Chen, 2010; Dobrynin et al., 2011). The diverse roles are regulated by substrate adaptors including Ufd1-Npl4 and a protein family containing UBX (ubiquitin-regulatory X) and UBX-like domains, which mediate binding to Cdc48/p97 (Schuberth and Buchberger, 2008; Kloppsteck et al., 2012). For example, using the heterodimeric Ufd1-Npl4 adaptor, Cdc48/p97 extracts Aurora B kinase from

F. Schwager, R. Holtackers, and J. Seiler contributed equally to this paper.

Correspondence to Monica Gotta: monica.gotta@unige.ch

Abbreviations used in this paper: DIC, differential interference contrast; NEBD, nuclear envelope breakdown; PCM, pericentriolar material; PN, pronucleus; UBX, ubiquitin-regulatory X.

The Rockefeller University Press $30.00
J. Cell Biol. Vol. 201 No. 4 559–575
www.jcb.org/cgi/doi/10.1083/jcb.201209107

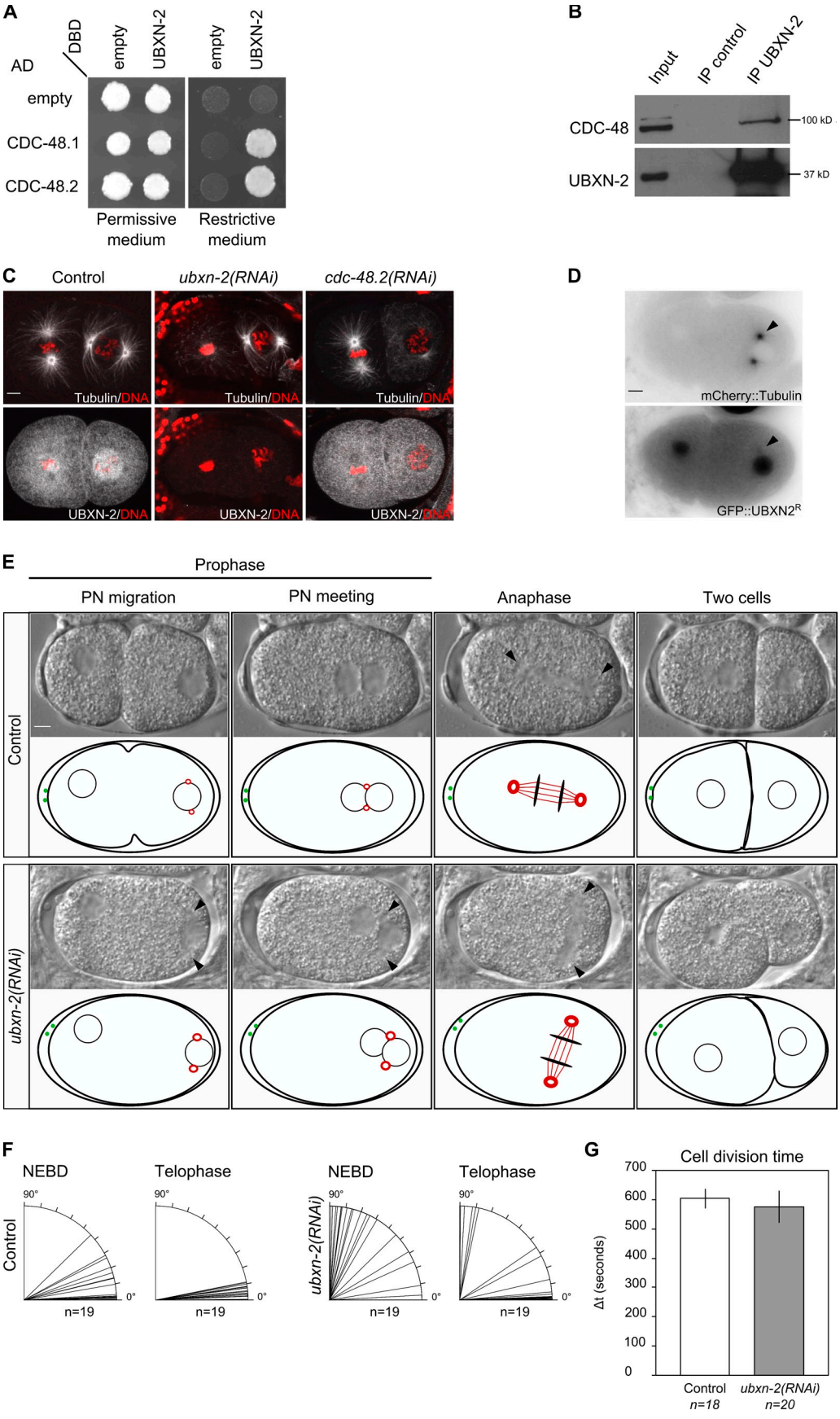

chromatin. This allows proper chromosome congression in human somatic cells (Dobrynin et al., 2011), chromatin decondensation and nuclear reformation at the end of mitosis in *Xenopus laevis* egg extracts and *Caenorhabditis elegans* embryos (Ramadan et al., 2007), and proper meiotic chromosome condensation in *C. elegans* (Sasagawa et al., 2012). Aurora B belongs to the family of Aurora kinases, which play crucial roles in cell division. Aurora B functions include regulation of chromosome condensation, microtubule–kinetochore interactions, spindle checkpoint, cytokinesis, and abscission (Steigemann et al., 2009; Lampson and Cheeseman, 2011; Santaguida et al., 2011). A second Aurora kinase, Aurora A, localizes to the spindle poles and the mitotic spindle and is required for centrosome maturation, mitotic entry, and bipolar spindle formation (Liu and Ruderman, 2006; Barr and Gergely, 2007).

In *Saccharomyces cerevisiae*, only a single Aurora form exists, called Ipl1. Ipl1 is also regulated by Cdc48, but in cooperation with an alternative adaptor, Shpl (Cheng and Chen, 2010). Mammals contain two orthologues of Shp1, p47 (NSFLC1) and p37 (UBXN2B), and *C. elegans* contains one orthologue, UBXN-2 (Schuberth and Buchberger, 2008). In metazoans p47 and p37 are involved in organelle biogenesis, including Golgi reformation at the end of mitosis (Uchiyama and Kondo, 2005; Uchiyama et al., 2006). Here we uncover a novel role for these cofactors, and show that human p37/p47 and their *C. elegans* orthologue UBXN-2 regulate centrosome function in prophase by limiting the recruitment of Aurora A.

Results

C. elegans ubxn-2(RNAi) one-cell embryos have spindle orientation defects

The *C. elegans* embryo is an ideal model to study cell division processes and spatiotemporal regulation of events. We set out to investigate if the orthologue(s) of p47 and p37 regulate cell division in this system.

In *C. elegans* there are six proteins containing UBX domains. Blast analysis with p37 and p47 showed that UBXN-2 is their closest orthologue. A reciprocal blast search using UBXN-2 identified p37 and p47 as the closest mammalian orthologues (Schuberth and Buchberger, 2008).

Consistent with the bioinformatic analysis and published data (Sasagawa et al., 2010), UBXN-2 interacted with the *C. elegans* orthologues of p97, CDC-48.1, and CDC-48.2 in yeast two-hybrid experiments (Fig. 1 A) and they coimmunoprecipitated from an embryonic extract (Fig. 1 B). UBXN-2 was both cytoplasmic and nuclear (Fig. 1 C; $n = 35$). This localization pattern was specific, as it was absent in UBXN-2–depleted embryos (Fig. 1 C; $n = 28$). Like other Cdc48/p97 adaptors (Mouysset et al., 2008), UBXN-2 nuclear localization depended on CDC-48 (Fig. 1 C; $n = 27$), indicating that UBXN-2 is a cofactor of CDC-48 in vivo. A GFP::UBXN-2 transgene that rescues UBXN-2 depletion was cytoplasmic and nuclear (Fig. 1 D). In metaphase to telophase embryos, GFP::UBXN-2 was also enriched around a region that corresponded, by differential interference contrast (DIC) microscopy, to the centrosomes/aster region. We therefore crossed the strain expressing GFP::UBXN-2 with a strain expressing α-tubulin fused to mCherry and confirmed that this region corresponds to centrosomes/asters (Video 1; $n = 10$). In 20% of embryos ($n = 59$) we could see a faint enrichment at the centrosomes area also in prophase (Fig. 1 D; Video 2).

We next investigated whether depletion of UBXN-2 caused embryonic defects. Up to 82% of *ubxn-2(RNAi)* embryos died (Table 1). To assess if depletion of UBXN-2 results in early embryonic defects, we performed time-lapse video microscopy. In control embryos (Fig. 1 E; Video 3; Table 1), fertilization drives completion of meiosis and establishment of the antero-posterior (a-p) polarity axis (Cowan and Hyman, 2004; Gönczy and Rose, 2005). During prophase, the anteriorly localized maternal pronucleus (PN) migrates toward the paternal one in the posterior, and the two pronuclei meet and centrate while rotating to align the centrosomes along the a-p axis (Video 3). Nuclear envelopes break down, the spindle forms in the center along the a-p axis (Fig. 1 F; average angle 6° ± 0.9), and it is subsequently pulled to the posterior. The two resulting cells are different in size, content, and fate.

In *ubxn-2(RNAi)* embryos the pronuclei met more posteriorly, their centration and rotation during prophase failed, and, as a consequence, the spindle elongated with an average angle of 51.3° ± 6.7 with the a-p axis after nuclear envelope broke down (Fig. 1, E and F; Video 4; Table 1). These defects and embryonic lethality were rescued by the expression of a RNAi-resistant GFP::UBXN-2 fusion (Table 1; GFP::UBXN-2^R strain). The incidence of the spindle orientation defect in *ubxn-2(RNAi)* embryos was ∼40% (Table 1). When depleting UBXN-2 in a heterozygous deletion mutant strain (the homozygous mutant made only 1– 10 embryos that developed partially inside the mother and died), 72% of embryos showed a spindle orientation defect (Table 1). The timing of cell division, calculated from completion of meiosis to nuclear envelope breakdown (NEBD), was unchanged in UBXN-2–depleted

Figure 1. **UBXN-2 interacts with CDC-48 and regulates spindle orientation in the one-cell *C. elegans* embryo.** (A) Yeast two-hybrid assay showing UBXN-2 interaction with *C. elegans* CDC-48.1 and CDC-48.2. Cells expressing the indicated proteins were spotted on permissive or restrictive media. Growth on restrictive medium indicates interaction. (B) CDC-48 coimmunoprecipitates with UBXN-2. (C) Localization of UBXN-2 by antibody staining in control, *ubxn-2(RNAi)*, and *cdc-48.2(RNAi)* two-cell embryos. UBXN-2 is cytoplasmic and nuclear in control embryos. (D) Still image from a wide-field time-lapse movie of a GFP::UBXN-2^R/mCherry::α-tubulin–expressing embryo (Video 1). Black arrowhead points to one of the centrosomes. (E) Top: DIC time-lapse recordings of control and *ubxn-2(RNAi)* embryos; bottom: schematic drawings. Black arrowheads point to centrosomes (red circles in the scheme). The black circles represent the pronuclei (referred to as PN in the figures), and the green dots represent the polar bodies. *ubxn-2(RNAi)* embryos had a weak or absent pseudocleavage. (F) Mitotic spindle orientation in one-cell embryos. Alignment of the centrosomes with the axis of polarity at NEBD and telophase, in control and *ubxn-2(RNAi)* embryos. Alignment along the antero-posterior axis corresponds to 0°. Each line represents an embryo. (G) Time interval (Δt = mean values in seconds ± SEM) from the exit of meiosis (appearance of the female pronucleus) to NEBD in the one-cell embryo, determined from DIC time-lapse movies. In all figures, numbers in italic (control-*RNAi*) indicate the number of embryos analyzed; anterior is on the left, posterior on the right. Bar, 5 µm.

Table 1. **Quantification of phenotypes**

Conditions	Embryonic lethality	Position at PN meeting	Spindle misorientation
			%
Wild type	0 (*n* = 217)	68.3 ± 0.7 (*n* = 11)	0 (*n* = 11)
ubxn-2(RNAi)	82.73 ± 4.97 (*n* = 274)	74.7 ± 1.4[e] (*n* = 33)	39.1 (*n* = 19)
GFP::UBXN-2[R]	0 (*n* = 279)	ND	0 (*n* = 16)
GFP::UBXN-2[R] *ubxn-2(RNAi)*	0 (*n* = 256)	66.4 ± 0.1 (*n* = 13)	0 (*n* = 10)
ubxn-2(ok1942)/+ [a]	51 ± 4 (*n* = 491)	67.7 ± 1.1 (*n* = 12)	0 (*n* = 9)
+/+ (VC362)[b]	47.7 ± 14.1 (*n* = 312)	67.4 ± 0.1 (*n* = 10)	0 (*n* = 10)
ubxn-2(ok1942)/+ ubxn-2(RNAi)	81.7 ± 10.4 (*n* = 348)	77 ± 1.4[d] (*n* = 36)	72[c] (*n* = 155)

Lethality is expressed as mean ± SEM. Pronuclear position at meeting is calculated as percentage of embryo length ± SEM.
[a]VC1450 strain. *n* = numbers of embryos analyzed.
[b]VC362 expresses the balancer used to balance *ubxn-2*(*ok1942*). The one-cell embryos behaved as wild-type embryos.
[c]The spindle orientation defects had a variable penetrance between experiments (50–90%).
[d]$P < 0.01$ compared to wild-type N2.
[e]$P < 0.05$ for the difference between wild-type and RNAi-treated embryos (*t* test).

embryos (Fig. 1 G). Furthermore, PAR-2 was localized at the posterior cortex in all one-cell *ubxn-2(RNAi)* embryos ($n = 21$) as in control ($n = 23$), indicating that the misoriented spindle was not the result of polarity defects (Fig. 2).

Our data show that UBXN-2 regulates spindle orientation in one-cell *C. elegans* embryos by controlling centration and rotation of the pronuclei–centrosome complex in prophase.

AIR-1 centrosomal accumulation is negatively regulated by UBXN-2

Regulation of astral microtubule dynamics and length is important for proper spindle positioning. For example, mutations that result in shorter microtubules, such as depletion of the TACC3 orthologue TAC-1 (Bellanger and Gönczy, 2003; Le Bot et al., 2003; Srayko et al., 2003) or the XMAP215 orthologue ZYG-9 (Matthews et al., 1998; Bellanger and Gönczy, 2003), both of which localize at centrosomes, result in short microtubules and mispositioned spindles. On the other side, a mutation in *let-711*, which results in higher levels of ZYG-9 at centrosomes and longer and more stable microtubules compared with wild type, also leads to misoriented spindles (DeBella et al., 2006). We therefore investigated whether proteins important for centrosome biogenesis and maturation (such as the Aurora A orthologue AIR-1 [Hannak et al., 2001; Toya et al., 2011], the cell-cycle kinase PLK-1 [Chase et al., 2000; Lee and Rhee, 2011], and the coil-coiled protein SPD-2 [O'Connell et al., 2000]) and for microtubule nucleation and polymerization (such as γ-tubulin [Strome et al., 2001], TAC-1, and ZYG-9) were properly localized in *ubxn-2(RNAi)* embryos. Quantification of the centrosomal levels of these proteins showed that AIR-1 was remarkably increased in UBXN-2–depleted embryos in prophase (Fig. 3 A; 1.5 ± 0.1-fold). ZYG-9, PLK-1, and SPD-2 were also enriched at this cell cycle time but to a lesser extent than AIR-1 (Fig. 3 A; 1.2 ± 0.08, 1.2 ± 0.07, and 1.1 ± 0.04-fold, respectively). AIR-1 increase was observed only in prophase (both early stages and pronuclear migration; Fig. S1 A) and not in metaphase (Fig. 3, B and C). The pool of AIR-1 essential for proper centrosome maturation is the kinase-active form of AIR-1 that is phosphorylated at Thr201 (Toya et al., 2011). Immunostaining of the kinase-active form of AIR-1 (P-AIR-1 antibodies; Toya et al., 2011) revealed that the levels of active AIR-1 are also enriched in *ubxn-2(RNAi)* embryos (Fig. 3, D and E).

Consistent with a role of UBXN-2 as cofactor of CDC-48, we observed an increase in AIR-1 accumulation at centrosomes in CDC-48–depleted embryos (Fig. 3, F and G). We conclude that UBXN-2 and CDC-48 limit AIR-1 accumulation at centrosomes in prophase.

UBXN-2 interacts with AIR-1 and influences AIR-1 mobile fraction in prophase

We next explored whether AIR-1 is a target of UBXN-2. We found that UBXN-2 and CDC-48 coimmunoprecipitated with AIR-1 from embryonic extracts (Fig. 4, A and B), suggesting

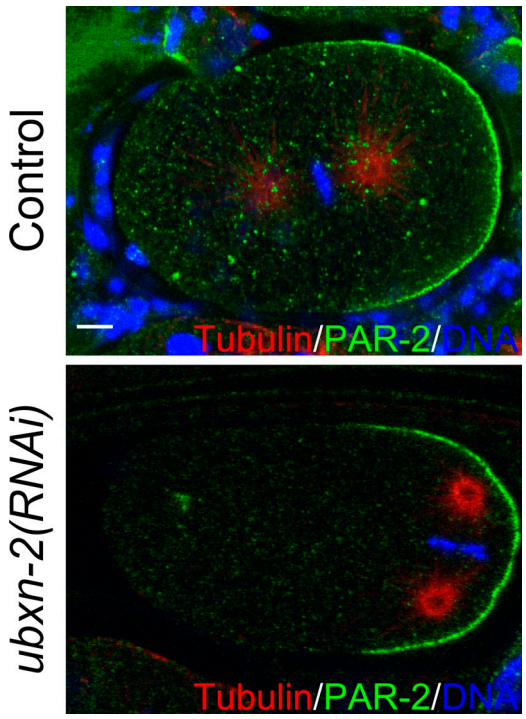

Figure 2. **Polarity is normal in *ubxn-2(RNAi)* embryos.** Control and *ubxn-2(RNAi)* one-cell embryos stained for α-tubulin, DNA, and PAR-2.

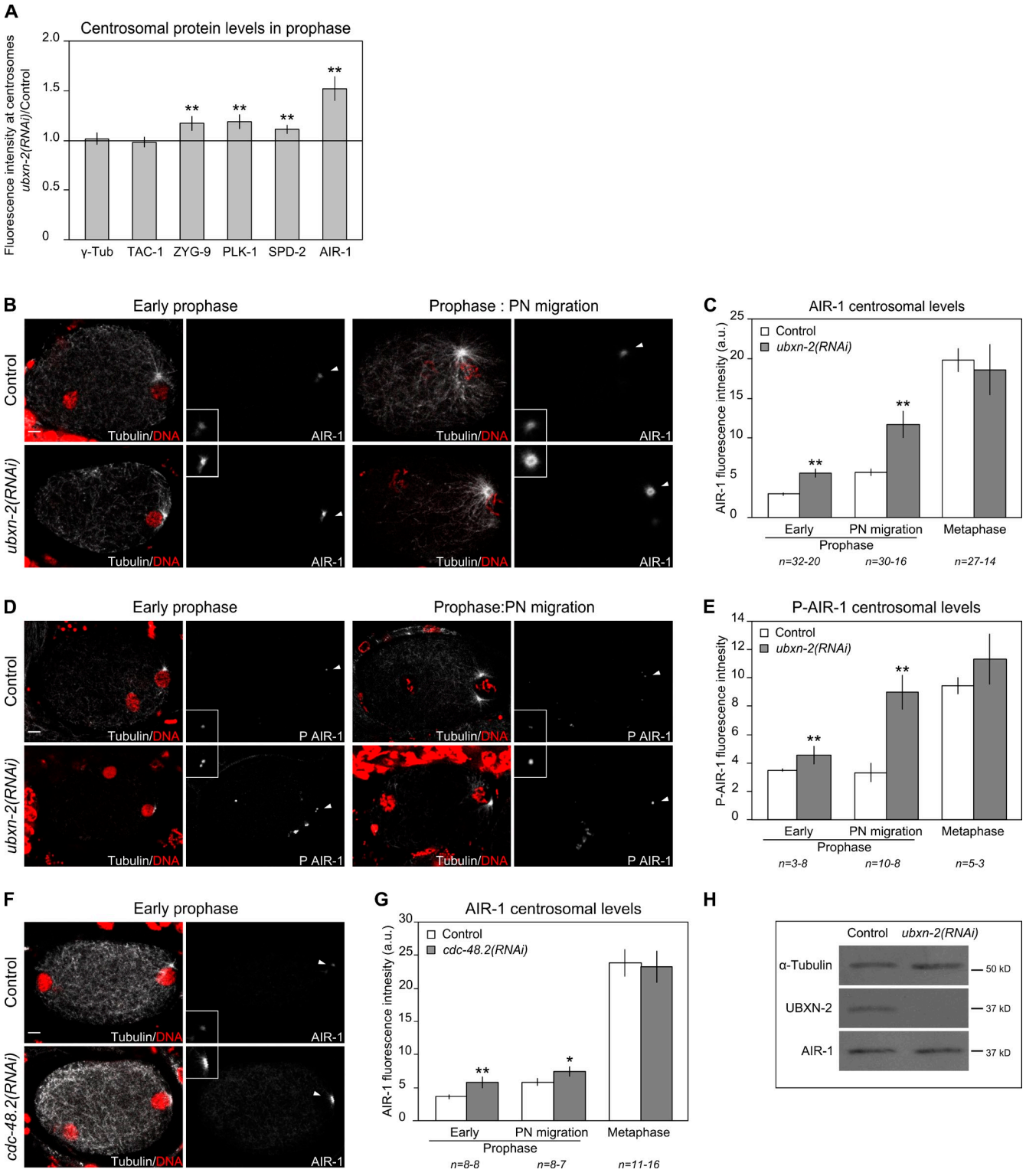

Figure 3. **AIR-1 centrosomal levels are higher in prophase *ubxn-2(RNAi)* embryos.** (A) Fold change (*ubxn-2(RNAi)* over control) of mean fluorescence intensities at centrosomes (±SEM) for the indicated proteins. The ratio = 1 is indicated by the horizontal bar. At least 30 embryos were analyzed for each protein. (B, D, and F) Embryos of the indicated genotype immunostained for α-tubulin and DNA, AIR-1 (B and F), and P-AIR1 (D). The insets present a magnified view (6.5 × 6.5 µm) of the centrosomes indicated by white arrowheads. (C, E, and G) Mean fluorescence intensity ± SEM at centrosomes of AIR-1 (C and G) or P-AIR-1 (E). (H) Western blot showing AIR-1 levels from embryonic extract of control and *ubxn-2(RNAi)* embryos. AIR-1 levels, normalized with tubulin, were 0.98 ± 0.1-fold (SEM, four independent experiments). *, $P < 0.05$; **, $P < 0.01$ for the difference between control and RNAi-treated embryos (*t* test).

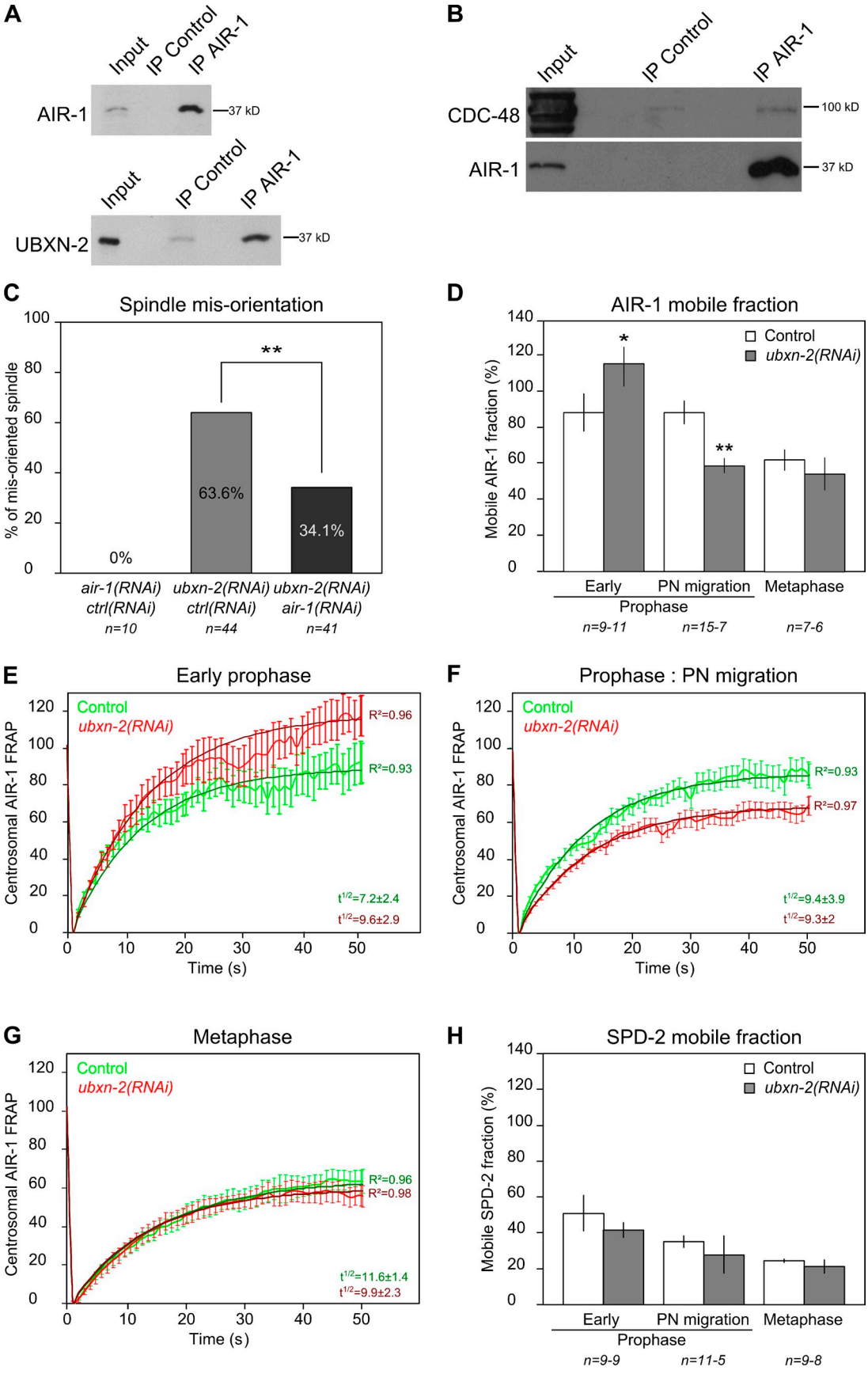

that UBXN-2 directly regulates AIR-1. Moreover, we confirmed this biochemical interaction at the functional level by depleting AIR-1 in *ubxn-2(RNAi)* embryos. In *ubxn-2(RNAi)* embryos, pronuclei meeting occurred more posteriorly compared with control (percentage of embryo length 77.3% ± 1.1; see also Table 1), centration and rotation failed, and the spindle elongated with an average angle of 45° ± 4.3 with the a-p axis. On the contrary, in ∼65% of *ubxn-2(RNAi);air-1(RNAi)* embryos pronuclear meeting occurred in average less posteriorly (62.7% ± 2.4 embryo length), centration and rotation occurred, and the spindle elongated with an average angle with the a-p axis of 7° ± 1.3 (Fig. 4 C; Fig. S2). The phenotypic rescue validates AIR-1 as a target of UBXN-2. However, embryonic lethality was not rescued (Fig. 4 C, legend), suggesting that UBXN-2 has additional targets, regulating spindle function or other processes, similar to other Cdc48/p97 adaptors (Cao et al., 2003; Ramadan et al., 2007).

Depletion of UBXN-2 did not result in a detectable change in AIR-1 total levels (Fig. 3 H), suggesting that UBXN-2 might regulate AIR-1 levels locally by controlling either recruitment to or removal from centrosomes. To test this we performed fluorescence recovery after photobleaching (FRAP) analysis of a centrosomal GFP::AIR-1 fusion. The percentage of fluorescence recovery at the end of the experiment is a quantitative readout of the fraction of mobile GFP::AIR-1 at centrosomes (Bastiaens and Pepperkok, 2000). The recovery half time ($t_{1/2}$) is the time required to reach 50% of the total net fluorescence recovered and is a measure of the exchange kinetics. The recovery half time of control and *ubxn-2(RNAi)* embryos were comparable at all cell cycle stages analyzed (Fig. 4, E–G). By contrast, the percentage of fluorescence recovery at centrosomes varied between control and *ubxn-2(RNAi)* embryos depending on the cell cycle stage analyzed. At pronuclear migration (prophase), 88% of GFP::AIR-1 was recovered at centrosomes in control embryos (Fig. 4 D). However, only 58% of GFP::AIR-1 was recovered in *ubxn-2(RNAi)* embryos, a value comparable to the one measured in metaphase in control embryos. This indicates that at pronuclear migration, in *ubxn-2(RNAi)* embryos, less photobleached GFP::AIR-1 can dissociate from centrosomes and exchange with the fluorescent cytoplasmic pool, suggesting that UBXN-2 is required to remove AIR-1 from centrosomes. We also performed FRAP of GFP::AIR-1 at centrosomes in early prophase, a time during which centrosomes actively accumulate pericentriolar material (PCM) and AIR-1. At this cell cycle stage, GFP::AIR-1 recovery in control was similar to the pronuclear migration stage. However, in *ubxn-2(RNAi)* embryos we observed a recovery of GFP::AIR-1 that appeared to be higher than control and that exceeded 100%. This can be explained by the fact that, at this cell cycle stage, the capacity of centrosomes to recruit AIR-1 increases in both control and *ubxn-2(RNAi)* embryos during the time of the measurement (50 s). The higher percentage of recovery in *ubxn-2(RNAi)* indicates that newly bound GFP::AIR-1 is not removed. This is consistent with the higher centrosomal levels of AIR-1 observed in *ubxn-2(RNAi*) embryos (Fig. 3 C) in early prophase and with a model in which UBXN-2 dissociates AIR-1 from centrosomes. In metaphase, the fluorescence recovery measured in control and *ubxn-2(RNAi)* embryos was similar, indicating that UBXN-2 has no role at this cell cycle stage.

SPD-2 was also weakly enriched at centrosomes upon UBXN-2 depletion (Fig. 3 A). We therefore performed a similar analysis on GFP::SPD-2 and found that, in contrast to GFP::AIR-1, the mobile fraction of SPD-2 was not affected by UBXN-2 depletion (Fig. 4 H).

These data suggest that UBXN-2 regulates centrosomal AIR-1 levels during mitotic progression by promoting its removal from centrosomes, in analogy to Cdc48/p97-mediated extraction in other processes (Meyer et al., 2012). Furthermore, our FRAP analysis on AIR-1 reveals that prophase centrosomes in UBXN-2–depleted embryos behave like metaphase centrosomes in control embryos.

UBXN-2 prevents premature formation of metaphase asters

AIR-1 is important to recruit key factors such as ZYG-9, TAC-1, and γ-tubulin to centrosomes (Hannak et al., 2001; Le Bot et al., 2003). Because we show that UBXN-2 regulates the timing of AIR-1 centrosomal accumulation, we analyzed the effect of UBXN-2 depletion on centrosome behavior and microtubule dynamics. We found that γ-tubulin, ZYG-9, and TAC-1 centrosomal levels were increased in prophase in UBXN-2–depleted embryos (Fig. 5, A–F), but to a lower extent than AIR-1 (Fig. 3 C). ZYG-9 increase was significant both in early prophase and during pronuclear migration, consistent with the general increase in prophase (Fig. 3 A; Fig. 5, A and B). γ-Tubulin and TAC-1, on the contrary, were only enriched during pronuclear migration, suggesting that these proteins are recruited at later stages of prophase, most likely in response to AIR-1 accumulation (Fig. 5, C–F; Hannak et al., 2001; Le Bot et al., 2003). Indeed, the enrichment during pronuclear migration is consistent with the strong increase of active AIR-1 detected at this cell cycle stage in *ubxn-2(RNAi)* embryos (Fig. 3 E).

Figure 4. **UBXN-2 regulates AIR-1 mobile fraction in prophase.** (A) AIR-1 coimmunoprecipitates with UBXN-2. The immunoprecipitation was split in two and ran in two independent gels because AIR-1 and UBXN-2 migrate at the same level (∼37 kD). (B) AIR-1 coimmunoprecipitates with CDC-48. (C) Quantification of the spindle misorientation phenotype of *ubxn-2(ok1942)/+* embryos depleted for UBXN-2, AIR-1, or both. *air-1(RNAi)* embryos did not form a spindle (Hannak et al., 2001). **, $P < 0.01$ for the difference between *ubxn-2(RNAi)* and *ubxn-2(RNAi)/air-1(RNAi)* embryos (χ^2 test). Embryonic lethality was 77.7% ± 6.54 for *ubxn-2(RNAi)*, 97.7% ± 3.42 for *air-1(RNAi)*, and 84.1% ± 4.76 for *ubxn-2(RNAi);air-1(RNAi)*. (D) Percentage of mobile fraction of AIR-1 estimated by FRAP. The strain used (OD142) expresses GFP::AIR-1. Histograms represent the mean (±SEM) of the five last points of each FRAP curve for the indicated cell cycle time. (E–G) FRAP results of control or *ubxn-2(RNAi)* GFP::AIR-1 at the indicated cell cycle time. The experimental mean values of FRAP ± SEM are presented in light green and red, respectively; the fitted curves are in dark green and red, respectively. Curves were fitted following the equation described in Materials and methods. The R^2 values indicate the correlation coefficient obtained by fitting experimental curves to the model. The $t_{1/2}$ represents FRAP half time. (H) Percentage of mobile fraction of SPD-2 estimated by FRAP, in control and *ubxn-2(RNAi)* embryos. The strain used (TH42) expresses GFP::SPD-2. Histograms represent the mean (±SEM) of the five last points of each FRAP curve for the indicated cell cycle time.

Figure 5. **UBXN-2 regulates centrosomal protein levels and centrosome behavior in a cell cycle–dependent manner.** (A, C, and E) Control and *ubxn-2(RNAi)* embryos stained for α-tubulin, DNA, ZYG-9 (A), TAC-1 (C), or γ-tubulin (E). The insets present a magnified view (6.5 × 6.5 µm) of the centrosomes indicated by white arrowheads. (B, D, and F) Mean fluorescence intensity at centrosomes ± SEM of ZYG-9 (B), TAC-1 (D), or γ-tubulin (F). (G) Analysis of centrosome volume throughout the cell cycle in control or *ubxn-2(RNAi)* embryos. The strain used (TH65) expresses YFP::α-tubulin. For each centrosome, the volume was normalized to the maximum; the histogram represents the mean ± SEM. (H) Mean growth speed ± SEM of astral microtubule speed in control or *ubxn-2(RNAi)*. The strain used (TH66) expresses EBP2::GFP. (I) Quantification of the number of astral microtubules longer than 3.75 µm per centrosome in control or *ubxn-2(RNAi)* embryos in prophase. (J) Quantification of the *ubxn-2(RNAi)* spindle misorientation phenotype observed by DIC in *ubxn-2(ok1942)/+* embryos depleted for UBXN-2, TAC-1, or both. **, P < 0.01 for the difference between *ubxn-2(RNAi)* and *ubxn-2(RNAi)/tac-1(RNAi)* embryos (χ^2 test).

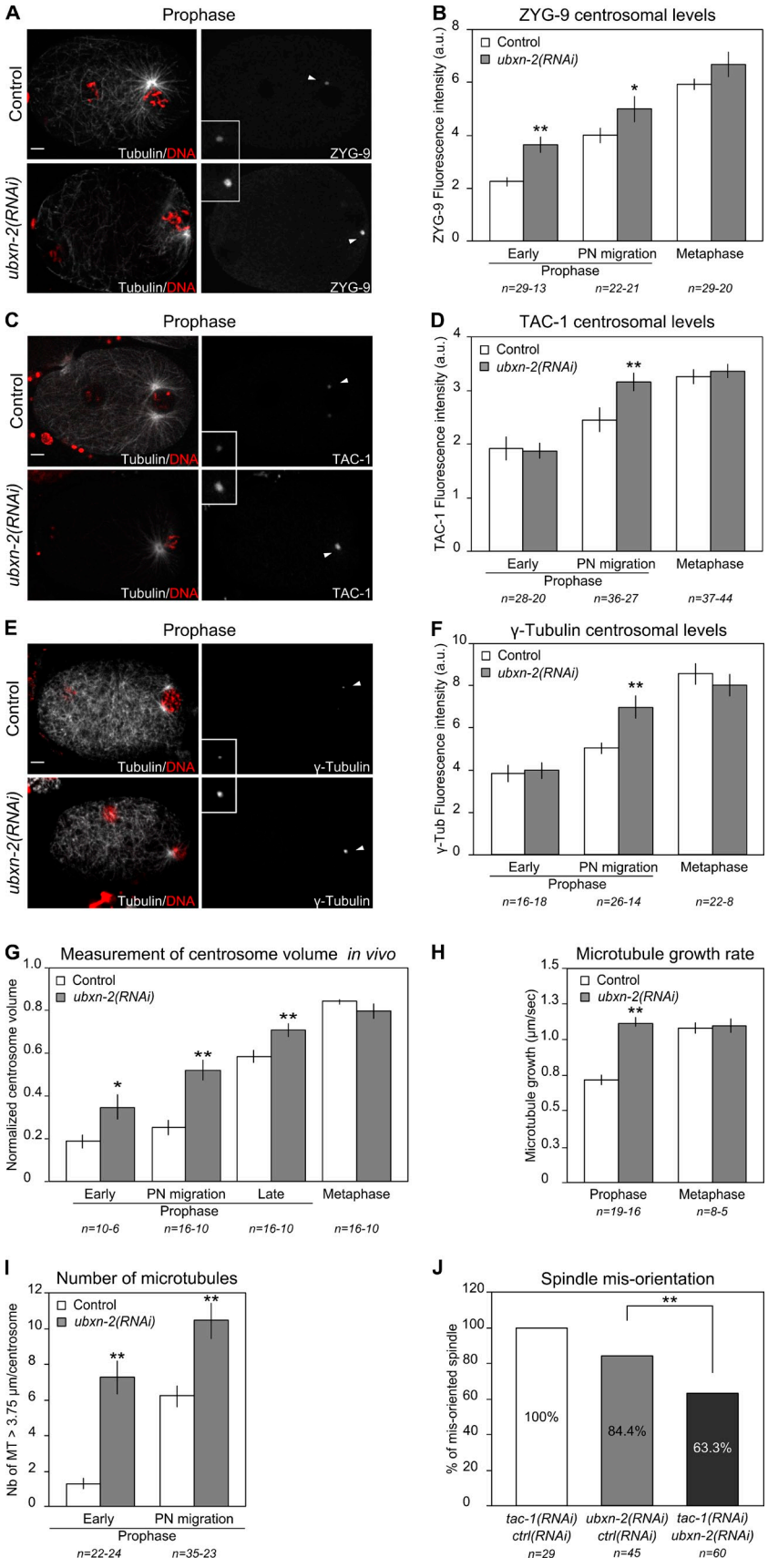

Centrosomes grow during their maturation, to reach their final size in metaphase (Decker et al., 2011). In vivo measurements of centrosome volume at different cell cycle stages showed that centrosomes in *ubxn-2(RNAi)* embryos were bigger than in control in prophase but not anymore in metaphase (Fig. 5 G; Fig. S3, A and B). Interestingly, a decrease in AIR-1 levels results in the opposite phenotype, centrosomes smaller than in wild type (Jaensch et al., 2010).

We next asked whether the growth rate of microtubules was affected by UBXN-2 depletion. Microtubule growth rate was higher in *ubxn-2(RNAi)* embryos compared with control in prophase (Fig. 5 H), consistent with the increase TAC-1 and ZYG-9 at this cell cycle time. Microtubule growth rate in prophase in *ubxn-2(RNAi)* embryos was comparable to metaphase in control ones. In metaphase embryos, microtubule growth rates in *ubxn-2(RNAi)* embryos were similar to control. We also observed an increased number of long microtubules (>3.75 µm) emanating from the centrosomes in *ubxn-2(RNAi)* embryos (Fig. 5 I; Fig. S3 C).

In UBXN-2–depleted embryos, therefore, microtubules grow faster and longer than in control. On the contrary, depletion of TAC-1 slows down polymerization rate and results in short microtubules. This leads to pronuclei meeting, centration and rotation defects, and ultimately misoriented spindles (Fig. 5 J; Bellanger and Gönczy, 2003; Le Bot et al., 2003; Srayko et al., 2003, 2005). Because depletion of TAC-1 and UBXN-2 have the opposite effect on microtubule growth rate, we weakly depleted TAC-1 in *ubxn-2(RNAi)* embryos. This resulted in a partial suppression of the *ubxn-2* spindle orientation defect. Indeed, in 37% of the co-depleted embryos, pronuclear meeting is in average comparable to control embryos (percentage of egg length 69.7% ± 1.8), and centration and rotation occurred, resulting in a spindle that elongates along the a-p axis (angle of 7.3° ± 1) compared with 16% of *ubxn-2(RNAi)* embryos (Fig. 5 J; Fig. S4; average angle of the spindle with the a-p axis 53° ± 4.5). Stronger depletion of TAC-1 in *ubxn-2(RNAi)* embryos resulted in 100% of embryos displaying the TAC-1 phenotype (unpublished data), indicating that *tac-1* is epistatic to *ubxn-2*.

Therefore, in UBXN-2–depleted embryos the centrosomal levels of microtubule dynamic regulators are increased and the growth rate of microtubules in prophase is comparable to the microtubule growth rate in metaphase in control embryos. This results in a spindle orientation defect that can be partially rescued by reducing microtubule polymerization rate and length.

p47 and p37 regulate centrosome behavior in early mitosis via Aurora A in human cells

We next investigated whether the function of UBXN-2 as a regulator of centrosome behavior in prophase and spindle orientation is conserved in human cells.

We first analyzed the localization of the human orthologues of UBXN-2, p37, and p47 (Fig. 6 A) during mitosis. In interphase cells p37 localizes at the Golgi and endoplasmic reticulum (Uchiyama et al., 2006), whereas p47 is mainly nuclear (Uchiyama et al., 2003). We used GFP fusions and found that both p37-GFP and p47-GFP were enriched at centrosomes from prophase to metaphase (Fig. 6 B).

We then depleted p37 and p47 by siRNAs (Uchiyama et al., 2006; Dobrynin et al., 2011) in HeLa cells expressing histone mCherry::H2B to monitor chromosome movements and GFP–α-tubulin to monitor formation of the mitotic spindle. Time-lapse imaging showed that cells co-depleted for p37 and p47 displayed a delay in centrosome separation (Fig. 6, C and D). Although in only 15% of control cells centrosomes failed to separate before NEBD, this occurred in 54% of p37/p47-depleted cells (Fig. 6 C). In 29% of cells depleted for p37 alone, the centrosomes were unseparated at NEBD, whereas depletion of p47 alone had no significant effect on centrosome separation (Fig. 6 C). These data suggest that p37 and p47 regulate the behavior of centrosomes during prophase. Moreover, they indicate that both cofactors have at least in part a redundant role in the control of centrosome separation and that p37 plays a prominent one.

We next tested whether this also correlated with changes in Aurora A levels at spindle poles during centrosome separation. We quantified the levels of Aurora A at different stages of centrosome separation in prophase cells (before NEBD; Fig. 6 F): Aurora A levels were similar in control and p37/p47-depleted cells before centrosome separation (centrosome–centrosome distance <3 µm) and after (centrosome–centrosome distance >9 µm). However, during centrosome separation (centrosome–centrosome distance 3–9 µm) there was a marked increase in Aurora A levels at centrosomes in p37/p47-depleted cells (Fig. 6, E and F). By contrast, and consistent with a prophase-specific regulation of Aurora A by p37/p47, we found no difference in centrosomal Aurora A levels in control versus p37/p47-depleted cells in metaphase (Fig. 6 G).

To test for a causal relationship between the two phenomena, we treated control or p37/47-depleted cells with the Aurora A inhibitor MLN8237 and recorded mitotic behavior by live-cell imaging (Fig. 6 C, right bars). Treatment with the inhibitor alone resulted in an increase in the percentage of cells with a centrosome separation delay compared with control cells (28% compared with 15% without inhibitor), consistent with a role for Aurora A in centrosome separation (Glover et al., 1995; Hoar et al., 2007; Cowley et al., 2009). In p37/p47-depleted cells, however, Aurora A inhibition decreased the percentage of cells with unseparated centrosomes at NEBD to 41% (from 54% in untreated cells). This indicated that Aurora A inhibition can partially rescue the centrosome separation defect of p37/p47-depleted cells, and that p37/p47 depletion has only a minor effect on centrosome separation when Aurora A is inhibited (41% compared with 28% in control cells).

We conclude that, as in *C. elegans*, p47 and p37 regulate centrosome behavior in early mitosis by limiting Aurora A localization to centrosomes.

p37 and p47 control spindle orientation

We next investigated whether p37 and p47 also regulate later stages of human cell division. In comparison to control cells we observed no significant delay in anaphase onset or chromosome alignment defects (Fig. 7 A); however, we noticed that in many cells the spindle rotated during prometaphase and metaphase (Fig. 7, A and B). In control cells the spindle generally oriented

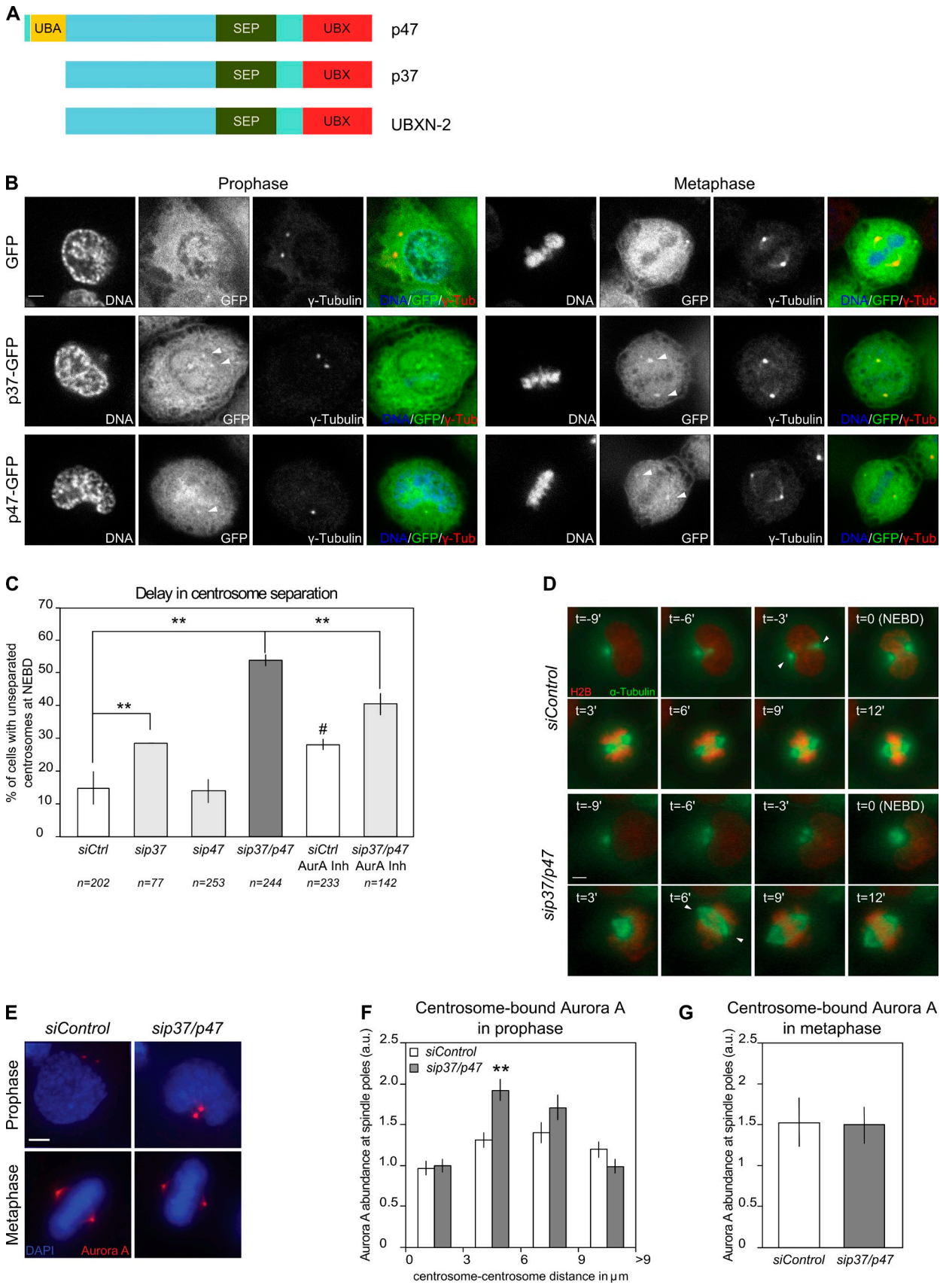

Figure 6. **Regulation of Aurora A centrosomal levels by UBX adaptors is conserved in human cells.** (A) Scheme of the main domains of UBXN-2, p37, and p47. UBA, ubiquitin-associating domain; UBX, ubiquitin regulatory X domain; SEP, Shp eyes-closed p47domain. (B) GFP-, p37-GFP–, or p47-GFP–expressing cells stained for γ-tubulin and DNA in prophase or metaphase. Centrosomal localization is observed in 85.7% of the p37-GFP cells (n = 56), 52.9%

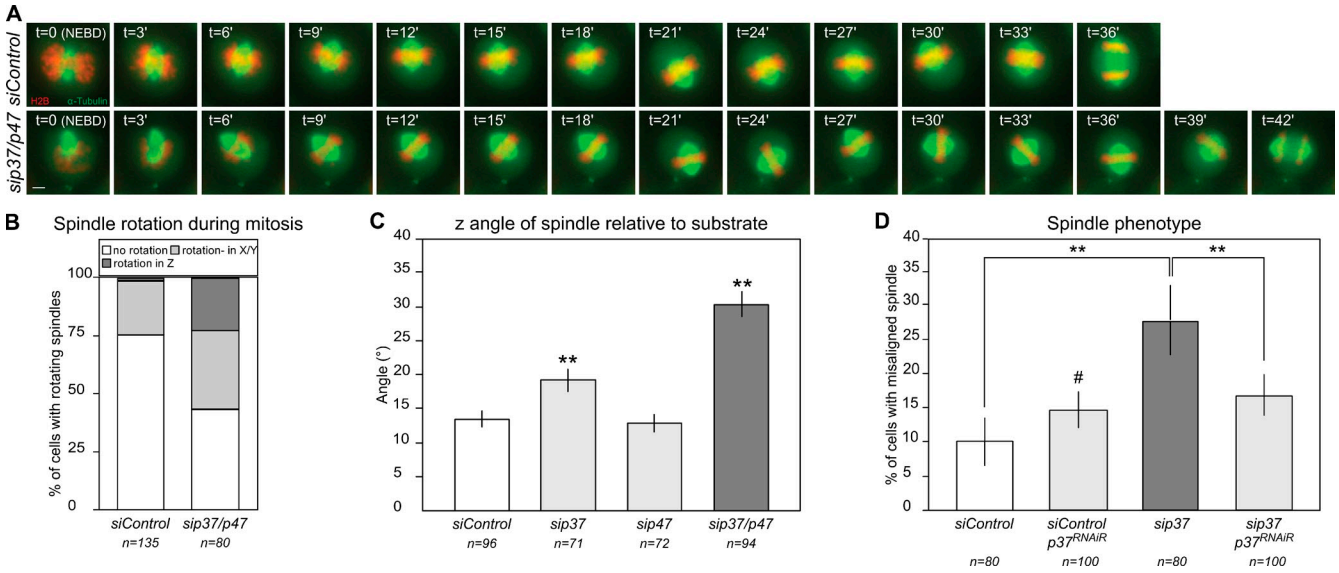

Figure 7. **p37 and p47 control spindle orientation in human cells.** (A) Time-lapse recording of HeLa Kyoto cells expressing mCherry::H2B and GFP::α-tubulin treated with either control siRNA or siRNA targeting p37 and p47. (B) Spindle rotation during mitosis, expressed as percentage of cells in control siRNA or p37/p47 siRNA–treated cells. The two distributions are significantly different (χ^2 test). (C) Mean spindle angle (α°) ± SEM in control siRNA, p37 siRNA, p47 siRNA, or p37 and p47 siRNA–treated HeLa cells. Measurements were done on fixed cells immunostained with α- and γ-tubulin. (D) Quantification of spindle rotation (z-axis) during mitosis expressed as percentage of cells, in control siRNA or p37 siRNA–treated cells induced or not for the expression of an siRNA-resistant form of p37 ($p37^{RNAiR}$). **, $P < 0.01$ (χ^2 test) for the indicated differences; #, $P < 0.01$ compared with *siCtrl*. Numbers of cells analyzed indicated in italic (*siCtrl-sip37/p47*).

parallel to the substrate, and in more than 75% of the cells the spindle was stable in both the x-y and the z axes. In contrast, after p37 and p47 co-depletion more than 50% of the cells had spindles that rotated either in the x-y or z axis (Fig. 7 B), suggesting a spindle orientation defect.

To confirm this result we measured the angle between the spindle and the substrate in fixed samples that were depleted of p37 and p47 individually or in combination (Fig. 7 C). Consistent with previous studies, in control-depleted cells we found an angle of 13.6° (Toyoshima and Nishida, 2007; Thoma et al., 2009). In contrast, in p37/p47 co-depleted cells, we found an average angle of 30.6°, which indicates randomization of spindle orientation. Depletion of p37 alone had a weaker effect (mean angle of 19.4°), whereas depletion of p47 alone had no significant effect on spindle orientation (mean angle of 13.06°), confirming the more prominent role of p37 in centrosome-dependent processes. Importantly, the phenotype was largely rescued by the expression of an siRNA-resistant p37 cDNA (Fig. 7 D; Fig. S5), excluding an off-target effect of the siRNAs. We therefore conclude that p37 and p47 control spindle orientation in human cells.

Discussion

Precise spatiotemporal regulation of events is crucial during cell division. Regulation of the localization and activity of mitotic kinases is one important way to achieve such precise coordination. Here we show that the Cdc48/p97 adaptors UBXN-2/p37/p47 are essential to limit centrosomal accumulation of the mitotic kinase AIR-1/Aurora A during cell division.

We find that in *C. elegans* the CDC-48 adaptor UBXN-2 is required to couple the timing of accumulation of PCM components at centrosomes with other events of cell division. When UBXN-2 is depleted, centrosomes mature too early and behave like metaphase centrosomes already in prophase. What drives this precocious accumulation of PCM components? Our data indicate that the mitotic kinase AIR-1 (Aurora A) is a target of UBXN-2. AIR-1 is required for several aspects of mitosis and it is essential for centrosome maturation (Hannak et al., 2001). Upon UBXN-2 depletion, higher amounts of AIR-1 localize to centrosomes in prophase, centrosomes recruit in excess other proteins essential for centrosomal function, are bigger, and microtubule growth rates are accelerated. In contrast to other situations in which centrosome size is also affected (DeBella et al., 2006; Song et al., 2008; Decker et al., 2011), centrosome size and AIR-1 levels are affected only during prophase in UBXN-2–depleted embryos and are again normal in metaphase. This indicates that UBXN-2 has a role in the coordination of centrosome maturation with cell cycle progression and not a role in size control.

This precocious accumulation of PCM components results in microtubules that grow faster and longer in prophase

of the p47-GFP cells ($n = 68$), and 26.2% of GFP cells ($n = 61$). The white arrowhead indicates the centrosomes in the GFP panels. (C) Percentage of cells with unseparated centrosomes at NEBD. **, $P < 0.01$ (χ^2 test) for the indicated differences; #, $P < 0.01$ compared with *siCtrl*. (D) Stills from time-lapse recording of HeLa Kyoto cells expressing mCherry::H2B and GFP::α-tubulin treated with either control siRNA or siRNA targeting p37 and p47. White arrowheads show the separated centrosomes. (E) Control or p37p47 siRNA–treated HeLa cells immunostained with DAPI and Aurora A. (F and G) Mean Aurora A fluorescence intensities at centrosomes in control or p37p47 siRNA–treated HeLa cells, in prophase (F) or metaphase (G).

and in a spindle alignment defect. How do increased levels of Aurora A result in longer microtubules and how can this lead to spindle orientation defect in metaphase? Beads coated with Aurora A have the ability to behave as a microtubule-organizing center (MTOC) and grow long astral microtubules in *Xenopus* extracts (Tsai and Zheng, 2005). The MTOC activity depends on the ability of Aurora A–coated beads to recruit additional microtubule nucleators and microtubule motors (Tsai and Zheng, 2005; Sardon et al., 2008). How exactly proteins enriched at centrosomes promote plus-end growth is still under intensive study, but work from several laboratories has shown a prominent role for the XMAP-215 microtubule polymerase (Brouhard et al., 2008; Slep, 2010; Al-Bassam and Chang, 2011).

In *C. elegans* one-cell embryos, alignment of the spindle along the antero-posterior axis depends on the rotation of the pronuclei/centrosome complex, which occurs in prophase. This rotation relies on the interaction of astral microtubules with motors such as dynein at the cortex and in the cytoplasm and depends on microtubule dynamics (McNally, 2013). Mutations that result either in shorter or more stable microtubules impair rotation and result in spindle orientation defects (Clark-Maguire and Mains, 1994; Bellanger and Gönczy, 2003; Le Bot et al., 2003; Srayko et al., 2003; Wright and Hunter, 2003; DeBella et al., 2006). Here we find that having an increased number of long astral microtubules in prophase also results in spindle orientation defects. *let-711* mutant embryos also have longer prophase microtubules and a centration and rotation defect (DeBella et al., 2006). An increased number of longer microtubules may result in improper or too numerous attachments to the cortex that interferes with centration and rotation of the pronuclei/centrosome complex, therefore resulting in orientation defects in metaphase. Consistent with this hypothesis, depletion of TAC-1 partially rescues the spindle orientation defect.

The regulation of Aurora A recruitment to centrosomes is conserved. Depletion of the UBXN-2 human orthologues p37 and p47 results in higher accumulation of Aurora A at centrosomes in prophase but not in metaphase. As a consequence centrosome separation timing is delayed, with more cells fully separating centrosomes only after the nuclear envelope has broken down. This can have functional implications, as cells in which centrosome separation is delayed until after NEBD are more prone to chromosome segregation errors (Kaseda et al., 2012; Mchedlishvili et al., 2012; Silkworth et al., 2012).

What are the mechanisms of Aurora A centrosomal level regulation? These adaptors could (1) regulate the number of Aurora A–binding sites on centrosomes; (2) inhibit the recruitment of Aurora A to centrosomes; and (3) promote the removal of Aurora A from centrosomes. If UBXN-2 would regulate the number of AIR-1–binding sites at centrosomes (1), AIR-1 levels should be higher at all cell cycle stages. If UBXN-2 would inhibit recruitment of AIR-1 to centrosomes (2), depletion of UBXN-2 would result in a higher percentage of fluorescence recovery also at pronuclear migration, as more GFP::AIR-1 would be recruited to centrosomes. One plausible model that fits our data is that UBXN-2 is required to remove AIR-1 from centrosomes (3). Indeed, during pronuclear migration (prophase) the percentage of fluorescence recovery is reduced in UBXN-2–depleted embryos, indicating that less centrosomal AIR-1 can exchange with the cytoplasmic pool. Interestingly, Cdc48/p97 uses ATP hydrolysis to undergo conformational changes, which generate a mechanical force used to disassemble protein complexes and remove proteins from DNA, membranes, or intracellular organelles. This activity has been defined as substrate extraction or segregation (Rape et al., 2001; Franz et al., 2011; Raman et al., 2011). We speculate that CDC-48/UBXN-2 extracts Aurora A from centrosomes in prophase to delay its accumulation, therefore coupling centrosome maturation timing with other events of mitosis. Consistent with a function of the complex in regulating AIR-1 levels locally at the centrosome, we observed an enrichment of UBXN-2, p37, and p47 at the centrosome area. It is interesting to note that Cdc48/p97 regulates local levels of Aurora B associated with chromatin at the end of mitosis with the Ufd1-Npl4 cofactors (Ramadan et al., 2007). This suggests that Cdc48/p97 may be a general regulator of Aurora kinases at the onset and at the end of mitosis via its different adaptors.

For some targets of Cdc48/p97 the process of extraction requires ubiquitination of the target protein. However, ubiquitin-independent mechanisms exist for Ship1 and p37 (Uchiyama et al., 2006; Krick et al., 2010). Consistent with a ubiquitin-independent role, neither UBXN-2 nor p37 have a UBA (ubiquitin binding) domain and the total levels of AIR-1 are unchanged upon depletion of UBXN-2. Future investigations will determine the exact molecular mechanisms of Aurora A dissociation from centrosomes by UBXN-2.

In human cells p47/p37 is required for membrane fusion and maintenance of Golgi during interphase (Uchiyama et al., 2006; Kaneko et al., 2010). Golgi-associated proteins are required for proper bipolar spindle formation (Colanzi et al., 2003) and the Golgi can control cell cycle progression. Indeed, inhibition of Golgi disassembly by injection of dominant-negative mutants of Golgi proteins (Persico et al., 2010) prevents Aurora A accumulation at centrosomes and results in a G2 arrest. However, stimulation of Golgi disassembly does not result in increased recruitment of Aurora A to centrosomes (Persico et al., 2010), indicating that p37 does not regulate Aurora A indirectly via the Golgi. Rather, we propose that in interphase and early mitosis p37 links these two processes by inhibiting recruitment of Aurora A to centrosomes on one side and Golgi disassembly on the other side.

How is the function of these adaptors temporally regulated? p37 and p47 are phosphorylated and inactivated by CDC2/CDK1 (Uchiyama et al., 2003; Kaneko et al., 2010). It is therefore possible that increasing CDK1 activity during mitosis results in increasing p37/p47 phosphorylation and inactivation, thus allowing Aurora A accumulation at centrosomes. Although UBXN-2 is a phosphoprotein (http://www.phosphopep.org/), the kinase(s) that phosphorylates UBXN-2 is unknown and CDK1 consensus phosphorylation sites are absent, suggesting that other mechanisms or other mitotic kinases may regulate the function of UBXN-2 in *C. elegans* embryos.

Depletion of p37 and p47 in mammalian cells also results in spindle orientation defects. Metaphase spindles are very dynamic and rotate in both the z and x-y axes, whereas in control

cells mitotic spindles are parallel to the substratum and their rotation in the x-y axis or in the z axis is minimal. Even p37/p47-depleted cells that separated centrosomes before NEBD, like the majority of control cells, display spindle orientation defects in metaphase, indicating that the orientation defect is not a consequence of the defect in centrosome separation in prophase. However, centrosomal levels of Aurora A are normal in metaphase. Therefore, these cofactors might have other targets that are important for proper control of spindle orientation in mammalian cells, consistent with our suppression data in *C. elegans*, suggesting that there are other targets of UBXN-2. An alternative possibility is that high centrosomal levels of Aurora A in prophase may affect a substrate that is important in metaphase to control spindle orientation. Those mechanisms will need to be further investigated to fully characterize the impact of Cdc48/p97 and its adaptors on the regulation of mitosis onset and spindle formation.

Materials and methods

Worm strains

Strains were handled using standard methods (Brenner, 1974). The strains used were wild-type N2, VC1450 (*ubxn-2*(ok1942)IV/nT1[qIs51]), VC362 (unc-5(e53) IV; dpy-11(e224) V/nT1[qIs51] (IV;V)), TH65 (YFP::α-tubulin; Kozlowski et al., 2007), OD142 (GFP::AIR-1; Portier et al., 2007), TH42 (GFP::SPD-2; Cowan and Hyman, 2004), TH66 (EBP-2::GFP; Srayko et al., 2005), ZU181 (GFP::UBXN-2^R), JA1558 (mCherry::α-tubulin; a gift from J. Arhinger (Gurdon Institute, Cambridge, England, UK; GFP::UBXN-2^R mCherry::α-tubulin).

Unless stated in the figure legends, *ubxn-2(RNAi)* was performed in *ubxn-2(ok1942)/+* worms, and the balancer strain (VC362) was used as a control.

RNAi

dsRNA targeting *ubxn-2* was produced as described previously (Zipperlen et al., 2001). Two non-overlapping templates were tested. One covers the first 325 bp, the other the last 583 bp of *ubxn-2* CDS (sjj_Y94H6A.9). Both dsRNAs gave the same phenotype and all subsequent experiments were done using the dsRNA targeting the last 583 bp. UBXN-2 depletion was performed by injecting dsRNA into L4 and incubating the worms at least 48 h at 22°C before analyzing the phenotype. As control dsRNA, we used *pde-5* (sjj_C32E12.2).

In *C. elegans*, depletion of both CDC-48.1 and CDC-48.2 can lead to meiotic arrest (Sasagawa et al., 2007), preventing analysis of the mitotic embryo. To overcome these defects, we used an RNAi that targets mainly CDC-48.2. Depletion of CDC-48.2 was done by injection, using the SP20G1 dsRNA (http://aquila.bio.nyu.edu/cgi-bin/rnaidb/ace/tree?name=SP20G1&class=RNAi_reagent) sequence as described in Piano et al. (2000).

For the double depletion of TAC-1 and UBXN-2 or AIR-1 and UBXN-2, worms injected with control *pde-5* dsRNA were fed on *tac-1* dsRNA-expressing bacteria (clone sjj_ Y54E2A.3) for 24 h at 22°C or *air-1* dsRNA-expressing bacteria (clone sjj_ K07C11.2) for 10 h at 22°C. Worms injected with *ubxn-2* dsRNA were fed on control bacteria (L4440) or *tac-1* dsRNA-expressing bacteria for 24 h at 22°C or *air-1* dsRNA-expressing bacteria for 10 h at 22°C. In all cases, proper depletion of UBXN-2 was assessed by immunostaining (see quantifications below).

Time-lapse microscopy

Image acquisition. Live imaging was conducted using a microscope (model DM6000; Leica) equipped with differential interference contrast (DIC) optics. Images were collected every 10 s using a 63×/NA 1.4 oil objective, a DFC 360 FX camera, and the LAS AF software (Leica). Embryos were mounted in 2% noble agar in egg buffer (118 mM NaCl, 48 mM KCl, 2 mM $CaCl_2$, 2 mM $MgCl_2$, and 25 mM Hepes, pH 7.5) and imaged at 22°C.

Centrosome alignment. To measure centrosome alignment with the polarity axis at NEBD and anaphase, the angle between a line dissecting the centrosomes and another following the antero-posterior axis was measured using the angle tool from ImageJ (National Institutes of Health).

Antibody production

Full-length *ubxn-2* CDS was cloned by gateway technology (Invitrogen) into pDEST-GST and the purified GST::UBXN2 protein was used to immunize rabbits (Charles River). The serum was purified by column using an MBP::UBXN-2 fusion (CnBr-activated Sepharose; Pharmacia).

For the production of the AIR-1 antibody, a peptide (Cys-Thr-Lys-Ser-Ser-Arg-Asn-Asn-Ser-Thr-Ala-Asn-Gln; Schumacher et al., 1998) was used for immunization (NeoMPS; PolyPeptide Laboratories). The serum was purified using a Sulfolink Immobolization kit for peptides (Thermo Fisher Scientific).

Yeast two-hybrid assay

The yeast two-hybrid assay was performed in the yeast strain MAV203 transformed according to the manufacturer's instructions with pDEST22 (Invitrogen) plasmids expressing transcriptional activation domain fusions, or pDEST32 (Invitrogen) plasmids expressing DNA binding domain fusions. The clones were spotted on leucine and tryptophan double dropout medium, and on leucine, tryptophan, and histidine triple dropout medium with 12.5 of 3AT.

Immunostaining, immunoprecipitation, and Western blot analyses

Immunostaining. Stainings were performed as described previously (Spilker et al., 2009), except for phospho–AIR-1(Toya et al., 2010). In brief, three-square (14 × 14 mm) epoxy autoclavable slides (Cel-line) were coated with 1% poly-L-lysine (in water) and 9 µl of egg buffer were pipetted on a square. 15–20 gravid worms were transferred on the egg buffer and cut open to release the embryos. A 22 × 40-mm coverslip was placed crosswise on the square to squash embryos until the nuclei were clearly visible. The slides were transferred on a metal block on dry ice for 20 min before flipping the coverslip (freeze-crack). The samples were then fixed for 20 min in cold methanol, blocked for 20 min in PBS/0.2% Tween 20 (PBST) and 1% BSA, and incubated overnight with primary antibodies at 4°C in a humid chamber. The day after, the slides were washed twice for 10 min in PBST, incubated with the secondary antibody solution including DAPI at room temperature for 45 min, washed twice for 5 min in PBST, and mounted in in Mowiol (6 g glycerol, 2.4 g Mowiol [475904; EMD Millipore], 6 ml H_2O, 12 ml 0.2 M Tris, pH 8.5, and 0.1% DABCO). For phospho–AIR-1, embryos were prepared as described above but were fixed for 30 s in cold methanol, and then 30 min in 3.2% paraformaldehyde, 0.24 M sorbitol prepared in 1× PEM (100 mM Pipes, 5 mM EDTA, and 5 mM $MgCl_2$). PEM was used instead of PBS for the washes. The following primary antibodies were used: anti–α-tubulin (mouse DM1A, 1:1,000; Sigma-Aldrich), anti-UBXN-2 (rabbit 1:100), anti–γ-tubulin (rabbit, 1:3,500, a gift from T. Hyman, Max Planck Institue of Molecular Cell Biology and Genetics, Dresden, Germany; Hannak et al., 2001), anti-TAC-1 (rabbit, 1:100, a gift from J. Arhinger; Le Bot et al., 2003), anti-ZYG-9 (rabbit, 1:100, a gift from P. Gönczy, EPFL, Lausanne, Switzerland; Gönczy et al., 2001), anti-AIR-1 (rabbit, 1:200), anti–phospho-AIR-1 (rabbit, 1:100; Toya et al., 2010), anti-PLK-1 (rabbit, 1:100; Noatynska et al., 2010), and anti–SPD-2 (rabbit, 1:6,000, a gift from T. Hyman; Decker et al., 2011). Alexa Fluor 488 anti–rabbit and Alexa Fluor 568 anti–mouse secondary antibodies were purchased from Molecular Probes. DNA was revealed using DAPI (Roche). Images were collected with a confocal microscope (LSM 510 Meta; Carl Zeiss) with a 63×/NA 1.4 oil objective (one single plane; Carl Zeiss) or an epifluorescence microscope (DM6000; Leica) with a 63×/NA 1.4 oil objective (Leica). Tubulin fluorescence was acquired so that the tubulin ring was never overexposed. Images were then processed with ImageJ. The maximum intensity threshold of the protein of interest in compared conditions was adjusted to the highest value. The minimum intensity threshold of DNA staining was adjusted for each showed picture to reduce the background.

Immunoprecipitation. Worms were grown on plates and embryos extracted by bleaching gravid adults (4.5% sodium hypochlorite and 0.5 M NaOH). Embryos were resuspended in immunoprecipitation buffer (IP buffer; 150 mM KCl, 50 mM Tris/HCl, pH 7.5, 5 mM $MgCl_2$, 1% Triton-X-100, 5% glycerol, 2 mM β-ME, and protease inhibitor cocktail [Roche]) and frozen in liquid nitrogen. To perform protein extraction, embryos were ground on dry ice using a mortar and pestle. The protein extract was centrifuged for 30 min at 14,000 rpm at 4°C. 5 µl protein G ultralink beads were mixed with an equivalent amount of either control or UBXN-2 or AIR-1 antibody at 4°C for 1 h. The beads were washed three times with IP buffer and incubated for 1 h at 4° with 450 µg of the embryonic extract. The beads were washed five times with IP buffer and boiled with SDS sample buffer for 5 min. Samples were then analyzed by Western blot.

Western blot. To obtain embryonic extract depleted of UBXN-2, 200 worms were injected with *ubxn-2* dsRNA and bleached 48 h after injection to recover embryos (4.5% sodium hypochlorite and 0.5 M NaOH).

Embryos were washed with 0.2% PBS/Tween and 0.01% Triton and resuspended in SDS sample buffer. SDS-PAGE and Western blot were performed following standard procedures. The antibodies used were diluted ten times more than for immunostainings. The anti–CDC-48 was a kind gift from T. Ogura (Institute of Molecular Embryology and Genetics, Kumamoto, Japan; Sasagawa et al., 2007). The Multi Gauge (Fujifilm) was used for quantification.

FRAP

The 2D-VisiFRAP System (Visitron Systems GmbH) was used to photobleach one centrosome. One image was taken before photobleaching, performed with one pulse of the 405-nm laser at 100% of the power. Acquisition was done with a microscope (Axio Imager.M2; Carl Zeiss) using an Evolve camera (Photometrics) and a 100×/NA 1.46 oil objective, and driven by MetaMorph software (Universal Imaging). The dimension of the bleached region was adjusted to the size of the centrosome. Acquisition was done for 251 frames, each of 0.2 s. Embryos were mounted in 2% noble agar in egg buffer, and imaged at 22°C.

Measurements were done following Hames et al. (2005). In brief, the fluorescence intensity at the bleached ROI (F1) was measured for each time point using ImageJ. The fluorescence intensity of an unbleached region of same area (F2) was also measured, in order to normalize the fluorescence loss due to acquisition: Fn = F1/F2. The background (Fb) intensity is considered as being the Fn value of the time point just after bleaching. To obtain the fluorescence intensity (Fi) at a time point n, this value was subtracted so that Fi = Fn − Fb. The fluorescence recovery after photobleaching at a time point was determined as the ratio of Fi over the Fi before photobleaching and expressed as 100% of prebleach value.

The FRAP curve obtained for each embryo was compared with a model ($f(t) = Vmax - Vmax.e^{(-t/koff)}$) (Aratyn et al., 2007). Curves with a correlation value lower than 70% ($R^2 < 0.7$) were excluded from the analysis. Those were mainly obtained from embryos where the bleached centrosome goes out of focus for several frames.

To evaluate the difference between control and *ubxn-2(RNAi)* embryos, the mean of the five last time points of each single curve was calculated. The p-value of a two-tailed Student's *t* test comparing the control and *ubxn-2(RNAi)* sets of data was used as readout of the significance of the differences observed.

Microtubule growth analysis

Imaging of the TH66 strain (expressing EBP-2::GFP) was done using the spinning confocal system Marianas SDC (Intelligent Imaging Innovative) mounted on a microscope (DMIRE2; Leica), with an EMCCD Evolve camera (Photometrics) and piloted by Slide Book software (Intelligent Imaging Innovative). Three Z-stacks of 0.5 µm at the centrosome level were acquired every 1.5 s, using a 63×/NA 1.4 objective and a binning of 2 × 2. Embryos were mounted in 2% noble agar in egg buffer and imaged at 22°C.

EBP-2::GFP dots were manually tracked using the ImageJ Manual Tracking plugin. Only comets that remained in the focal plane for at least three frames were tracked. At least five microtubules per embryo were analyzed.

4D analysis

Embryos of TH65 strain were imaged with a confocal spinning disk microscope (CSU 21; Yokogawa Corporation of America) equipped with a 100×/NA 1.4 oil objective, an EMCCD camera (iXon EM+; Andor Technology) and piloted with the iQ software (Andor Technology). Z-stacks (10 slices) were acquired every 8 s from fluorescent zygotes. Multidimensional data were treated and analyzed with Imaris 7.2.3 64-bit software (Bitplane). The size of fluorescently labeled centrosomes was automatically calculated over time using a thresholding-based segmentation. Then, all volumes from a same sequence were normalized with the highest volume observed over time.

Imaging of GFP::UBXN-2 mCherry::α-tubulin

For imaging of the prophase, embryos of the ZU210 strain were imaged with a microscope (Axio Imager.M2; Carl Zeiss) using a 100×/NA 1.46 oil objective and an Evolve EMCCD camera (Photometrics). Images were collected every 10 s using MetaMorph software (Universal Imaging), and then processed with ImageJ.

For imaging of later stages, embryos of the ZU210 strain were imaged using a microscope (DM6000; Leica). Images were collected every 15 s for a few planes of 1-µm distance around the centrosomes using a 63×/NA 1.4 oil objective, a camera (DFC 360 FX; Leica), and the LAS AF software (Leica). Stacks were deconvolved with Huygens Essential software (v.4.1.0; Scientific Volume Imaging). In both cases, embryos were mounted in 2% noble agar in egg buffer and imaged at 22°C.

Quantification of images

For the measurement of fluorescence intensities, the first division was arbitrarily divided in four stages: early prophase, pronuclear migration, end of prophase, and metaphase.

Fluorescence intensities. Quantifications were done using the LAS AF software. The maximum fluorescence intensity at centrosomes and the mean intensity of an ROI in the cytoplasm were measured. The level of fluorescence at centrosome was calculated as the ratio of centrosomal over cytoplasmic fluorescence intensities.

For the double depletion experiments, intensity of UBXN-2 staining was calculated as the ratio of the mean intensity of an ROI in the cytoplasm of one, two, or four cells embryos over the mean intensity of a similar ROI outside the cell.

Number of microtubules. To estimate the number of astral microtubules, a 7.5-µm-diameter circle was drawn with ImageJ around the centrosome, and the number of microtubules longer than the 3.75-µm limit was counted. To avoid the nucleus from which astral microtubules are excluded and the cortex that limits microtubule growth, only the inner quadrant was analyzed (Fig. S3 C, dotted quadrant). The measurements were done on confocal images taken at the mid-centrosome plane.

HeLa cells

Human tissue culture, siRNA, and drug treatments. All cells were grown in DMEM containing 10% FCS, 100 U/ml penicillin, and 100 mg/ml streptomycin at 37°C with 5% CO_2 in a humidified incubator. HeLa EGFP–α-tubulin/H2B-mCherry were grown under additional selection (0.2 µg/ml of G418 and 0.5 µg/ml of puromycin; Mchedlishvili et al., 2012). Live-cell imaging experiments were performed at 37°C in Lab-Tek II chambers (Thermo Fisher Scientific) with Leibovitz L-15 medium containing 10% FCS. Short RNAi nucleotides against control (Mchedlishvili et al., 2012), p37 (5′-CUCCAGAAGAGGAGGAUAA-3′; Uchiyama et al., 2006), and p47 (5′-AGCCAGCUCUUCCAUCUUA-3′; Dobrynin et al., 2011) were transfected as described previously (Elbashir et al., 2001) and analyzed 48 h after transfection. For drug treatments, cells were treated for 48 h with 20 nM of the Aurora A inhibitor MLN8237.

Restoration experiment and expression of GFP fusions. A stable HeLa Kyoto cell line with doxycycline-inducible expression of mouse p37 was generated based on the Flip-In system (Invitrogen; parental cells kindly provided by U. Kutay, ETH Zurich, Zurich, Switzerland). For transfection, mouse p37 cDNA (IMAGE clone 30637967) was amplified by PCR (primer forward: 5′-TTGACCTGGATCCATGGCGGAGGGTGGCCGT-3′; primer backward: 5′-AGTTCATGGATCCTTTTAGCTGTTGGAGTATCACA-3′) and cloned into the BamHI site of pcDNA5/FRT/TO (Invitrogen) with a sequence encoding for a C-terminal 3×HA-strep tag. For restoration experiments, cells were transfected with 30 nM p37 siRNA using Lipofectamine RNAiMAX. A nonsilencing siRNA (5′-UUCUCCGAACGUGUCACGUdTdT-3′) was used as control. Expression of siRNA-resistant p37 was induced by doxycycline 8–14 h after siRNA transfection, and cells were fixed after 48 h and stained for γ-tubulin (1:200, clone GTU-88, catalog no. T6557; Sigma-Aldrich) and DNA. The spindle orientation in anaphase cells was scored visually based on the position of spindle poles and sister chromatid masses with respect to the focal plane.

To express GFP fusions, the mouse p37 cDNA (IMAGE clone 30637967) and rat p47 cDNA (Meyer et al., 2000) were cloned into the BamHI site of pcDNA5/FRT/TO (Invitrogen) with a sequence encoding for a C-terminal GFP tag. HeLa Kyoto cells were transfected with GFP-tagged p37, p47, or with GFP using jetPEI (Polyplus Ttransfection). Cells were fixed after 48 h with methanol at −20°C for 6 min and stained for γ-tubulin (1:200, clone GTU-88; Sigma-Aldrich) and DNA (DAPI). Confocal images were taken with a microscope (Eclipse Ti; Nikon) equipped with a 100×/NA 1.49 oil objective, a confocal unit (CSU-X1; Yokogawa Corporation of America), and an EMCCD camera (iXon X3; Andor Technology) driven by iQ2 software (Andor Technology).

p37 antibody. Polyclonal antisera to p37 were raised in rabbits against a GST fusion of mouse p37 (animal no. 20880; BioGenes) and affinity purified. The antibody was used in Western blot at a dilution of 1:100.

Fixed and live-cell imaging. Cells were fixed with methanol at −20°C for 6 min. Live-cell imaging of HeLa EGFP–tubulin/H2B-mRed was carried for 8 h on a DeltaVision microscope (Applied Precision) using a 40×/NA 1.3 oil objective and a camera (CoolSNAP HQ; Roper Scientific) with a

sampling rate of 3 min, recording at each time point 8 z-stacks at a distance of 0.2 µm using Softworx software (Applied Precision).

The following primary antibodies were used: rabbit anti–Aurora A (1:500; Novus Biologicals) and rabbit anti-tubulin (1:1,000; Sigma-Aldrich). Cross-adsorbed secondary antibodies were used (Invitrogen). 3D image stacks of mitotic cells were acquired in 0.2-µm steps using 60× or 100×/NA 1.4 oil objectives on a DeltaVision microscope (Applied Precision) equipped with a camera (CoolSNAP HQ; Roper Scientific). The 3D image stacks were acquired and deconvolved with SoftWorx (Applied Precision). For quantitative Aurora A measurements and for centrosome distance measurements, signals were determined and quantified with SoftWorx. Spindle angles were measured as described previously (Thoma et al., 2009). In brief, a series of z-sections of 0.2 µm encompassing the two centrosomes was taken. The distance between the two centrosomes in z, as well as their projected distance, were calculated and the two values were used to calculate the angle of the spindle with the substrate.

Statistical analysis

The data presented are representative of at least three independent experiments. A two-tailed Student's *t* test was used to compare two sets of data. A Chi^2 test was used to assess the difference between two sets of qualitative distribution.

Online supplemental material

Fig. S1 is methodological and supports the main figures. It illustrates the cell cycle stages analyzed from fixed or live embryos. Fig. S2 supports the data in Fig. 4 C and shows that UBXN-2 depletion is not affected by co-depletion of AIR-1. Fig. S3 is a methodological figure that supports Fig. 5, G and I. It exemplifies how centrosome volume was measured from time-lapse movies and how the number of long astral microtubules was counted. Fig. S4 supports the data in Fig. 5 J and shows that UBXN-2 depletion is not affected by co-depletion of TAC-1. Fig. S5 is related to Fig. 5 D and shows the expression of the RNAi-resistant form of p37 in HeLa cells. Videos 1 and 2 are related to Fig. 1, C and D. They show the localization of a GFP::UBXN-2 and mCherry::α-tubulin during the first division of a *C. elegans* embryo. Videos 3 and 4 are related to Fig. 1, E and F, and illustrate the phenotype of *ubxn-2(RNAi)* embryos (Video 4) compared with control (Video 3). Online supplemental material is available at http://www.jcb.org/cgi/content/full/jcb.201209107/DC1.

We thank T. Hyman, P. Gonczy, J. Arhinger, T. Ogura, K. Oegema, and D.G. Moerman for reagents and strains, and the Viollier Laboratory for the use of their 2D-VisiFRAP system. We are grateful to M. Prouteau for his advice about statistical analysis, and to laboratory members for helpful discussions. We thank the Bioimaging Core facility of the Medical Faculty, the NCCR Frontiers in Genetics Bioimaging Platform for their help with microscopy. Some strains used in this work were provided by the *Caenorhabditis* Genetics Center (funded by the NIH National Center of Research Resources).

This work was supported by a grant from the Swiss National Science Foundation, the NCCR Chemical Biology, and by funding from the University of Geneva to M. Gotta. E. Kress was also funded by the Ernst & Lucie Schmidheiny, the Ernest Boninchi, and the Novartis foundations. P. Meraldi and R. Holtackers were funded by ETH Zurich and the Swiss National Science Foundation. A. Sugimoto was funded by JSPS KAKENHI (19671003) and the Funding Program for Next Generation World-Leading Researchers (LS006). H. Meyer was funded by Deutsche Forschungsgemeinschaft grant ME 1626/3-1.

Submitted: 18 September 2012
Accepted: 6 March 2013

References

Al-Bassam, J., and F. Chang. 2011. Regulation of microtubule dynamics by TOG-domain proteins XMAP215/Dis1 and CLASP. *Trends Cell Biol.* 21:604–614. http://dx.doi.org/10.1016/j.tcb.2011.06.007

Aratyn, Y.S., T.E. Schaus, E.W. Taylor, and G.G. Borisy. 2007. Intrinsic dynamic behavior of fascin in filopodia. *Mol. Biol. Cell*. 18:3928–3940. http://dx.doi.org/10.1091/mbc.E07-04-0346

Barr, A.R., and F. Gergely. 2007. Aurora-A: the maker and breaker of spindle poles. *J. Cell Sci.* 120:2987–2996. http://dx.doi.org/10.1242/jcs.013136

Bastiaens, P.I., and R. Pepperkok. 2000. Observing proteins in their natural habitat: the living cell. *Trends Biochem. Sci.* 25:631–637. http://dx.doi.org/10.1016/S0968-0004(00)01714-X

Bellanger, J.M., and P. Gönczy. 2003. TAC-1 and ZYG-9 form a complex that promotes microtubule assembly in *C. elegans* embryos. *Curr. Biol.* 13:1488–1498. http://dx.doi.org/10.1016/S0960-9822(03)00582-7

Brenner, S. 1974. The genetics of *Caenorhabditis elegans*. *Genetics*. 77:71–94.

Brouhard, G.J., J.H. Stear, T.L. Noetzel, J. Al-Bassam, K. Kinoshita, S.C. Harrison, J. Howard, and A.A. Hyman. 2008. XMAP215 is a processive microtubule polymerase. *Cell*. 132:79–88. http://dx.doi.org/10.1016/j.cell.2007.11.043

Cao, K., R. Nakajima, H.H. Meyer, and Y. Zheng. 2003. The AAA-ATPase Cdc48/p97 regulates spindle disassembly at the end of mitosis. *Cell*. 115:355–367. http://dx.doi.org/10.1016/S0092-8674(03)00815-8

Chase, D., C. Serafinas, N. Ashcroft, M. Kosinski, D. Longo, D.K. Ferris, and A. Golden. 2000. The polo-like kinase PLK-1 is required for nuclear envelope breakdown and the completion of meiosis in *Caenorhabditis elegans*. *Genesis*. 26:26–41. http://dx.doi.org/10.1002/(SICI)1526-968X(200001)26:1<26::AID-GENE6>3.0.CO;2-O

Cheng, Y.L., and R.H. Chen. 2010. The AAA-ATPase Cdc48 and cofactor Shp1 promote chromosome bi-orientation by balancing Aurora B activity. *J. Cell Sci.* 123:2025–2034. http://dx.doi.org/10.1242/jcs.066043

Clark-Maguire, S., and P.E. Mains. 1994. Localization of the mei-1 gene product of *Caenorhabditis elegans*, a meiotic-specific spindle component. *J. Cell Biol.* 126:199–209. http://dx.doi.org/10.1083/jcb.126.1.199

Colanzi, A., C. Suetterlin, and V. Malhotra. 2003. Cell-cycle-specific Golgi fragmentation: how and why? *Curr. Opin. Cell Biol.* 15:462–467. http://dx.doi.org/10.1016/S0955-0674(03)00067-X

Cowan, C.R., and A.A. Hyman. 2004. Asymmetric cell division in *C. elegans*: cortical polarity and spindle positioning. *Annu. Rev. Cell Dev. Biol.* 20:427–453. http://dx.doi.org/10.1146/annurev.cellbio.19.111301.113823

Cowley, D.O., J.A. Rivera-Pérez, M. Schliekelman, Y.J. He, T.G. Oliver, L. Lu, R. O'Quinn, E.D. Salmon, T. Magnuson, and T. Van Dyke. 2009. Aurora-A kinase is essential for bipolar spindle formation and early development. *Mol. Cell. Biol.* 29:1059–1071. http://dx.doi.org/10.1128/MCB.01062-08

DeBella, L.R., A. Hayashi, and L.S. Rose. 2006. LET-711, the *Caenorhabditis elegans* NOT1 ortholog, is required for spindle positioning and regulation of microtubule length in embryos. *Mol. Biol. Cell*. 17:4911–4924. http://dx.doi.org/10.1091/mbc.E06-02-0107

Decker, M., S. Jaensch, A. Pozniakovsky, A. Zinke, K.F. O'Connell, W. Zachariae, E. Myers, and A.A. Hyman. 2011. Limiting amounts of centrosome material set centrosome size in *C. elegans* embryos. *Curr. Biol.* 21:1259–1267. http://dx.doi.org/10.1016/j.cub.2011.06.002

Dobrynin, G., O. Popp, T. Romer, S. Bremer, M.H. Schmitz, D.W. Gerlich, and H. Meyer. 2011. Cdc48/p97-Ufd1-Npl4 antagonizes Aurora B during chromosome segregation in HeLa cells. *J. Cell Sci.* 124:1571–1580. http://dx.doi.org/10.1242/jcs.069500

Elbashir, S.M., J. Harborth, W. Lendeckel, A. Yalcin, K. Weber, and T. Tuschl. 2001. Duplexes of 21-nucleotide RNAs mediate RNA interference in cultured mammalian cells. *Nature*. 411:494–498. http://dx.doi.org/10.1038/35078107

Franz, A., M. Orth, P.A. Pirson, R. Sonneville, J.J. Blow, A. Gartner, O. Stemmann, and T. Hoppe. 2011. CDC-48/p97 coordinates CDT-1 degradation with GINS chromatin dissociation to ensure faithful DNA replication. *Mol. Cell*. 44:85–96. http://dx.doi.org/10.1016/j.molcel.2011.08.028

Fröhlich, K.U., H.W. Fries, M. Rüdiger, R. Erdmann, D. Botstein, and D. Mecke. 1991. Yeast cell cycle protein CDC48p shows full-length homology to the mammalian protein VCP and is a member of a protein family involved in secretion, peroxisome formation, and gene expression. *J. Cell Biol.* 114:443–453. http://dx.doi.org/10.1083/jcb.114.3.443

Glover, D.M., M.H. Leibowitz, D.A. McLean, and H. Parry. 1995. Mutations in aurora prevent centrosome separation leading to the formation of monopolar spindles. *Cell*. 81:95–105. http://dx.doi.org/10.1016/0092-8674(95)90374-7

Gönczy, P., and L.S. Rose. 2005. Asymmetric cell division and axis formation in the embryo. *WormBook*. 15:1–20. http://dx.doi.org/10.1895/wormbook.1.30.1

Gönczy, P., J.M. Bellanger, M. Kirkham, A. Pozniakowski, K. Baumer, J.B. Phillips, and A.A. Hyman. 2001. zyg-8, a gene required for spindle positioning in *C. elegans*, encodes a doublecortin-related kinase that promotes microtubule assembly. *Dev. Cell*. 1:363–375. http://dx.doi.org/10.1016/S1534-5807(01)00046-6

Hames, R.S., R.E. Crookes, K.R. Straatman, A. Merdes, M.J. Hayes, A.J. Faragher, and A.M. Fry. 2005. Dynamic recruitment of Nek2 kinase to the centrosome involves microtubules, PCM-1, and localized proteasomal degradation. *Mol. Biol. Cell*. 16:1711–1724. http://dx.doi.org/10.1091/mbc.E04-08-0688

Hannak, E., M. Kirkham, A.A. Hyman, and K. Oegema. 2001. Aurora-A kinase is required for centrosome maturation in *Caenorhabditis elegans*. *J. Cell Biol.* 155:1109–1116. http://dx.doi.org/10.1083/jcb.200108051

Hoar, K., A. Chakravarty, C. Rabino, D. Wysong, D. Bowman, N. Roy, and J.A. Ecsedy. 2007. MLN8054, a small-molecule inhibitor of Aurora A, causes spindle pole and chromosome congression defects leading to

aneuploidy. *Mol. Cell. Biol.* 27:4513–4525. http://dx.doi.org/10.1128/MCB.02364-06

Jaensch, S., M. Decker, A.A. Hyman, and E.W. Myers. 2010. Automated tracking and analysis of centrosomes in early *Caenorhabditis elegans* embryos. *Bioinformatics*. 26:i13–i20. http://dx.doi.org/10.1093/bioinformatics/btq190

Kaneko, Y., K. Tamura, G. Totsukawa, and H. Kondo. 2010. Phosphorylation of p37 is important for Golgi disassembly at mitosis. *Biochem. Biophys. Res. Commun.* 402:37–41. http://dx.doi.org/10.1016/j.bbrc.2010.09.097

Kaseda, K., A.D. McAinsh, and R.A. Cross. 2012. Dual pathway spindle assembly increases both the speed and the fidelity of mitosis. *Biol Open*. 1:12–18. http://dx.doi.org/10.1242/bio.2011012

Kloppsteck, P., C.A. Ewens, A. Förster, X. Zhang, and P.S. Freemont. 2012. Regulation of p97 in the ubiquitin-proteasome system by the UBX protein-family. *Biochim. Biophys. Acta*. 1823:125–129. http://dx.doi.org/10.1016/j.bbamcr.2011.09.006

Kozlowski, C., M. Srayko, and F. Nedelec. 2007. Cortical microtubule contacts position the spindle in *C. elegans* embryos. *Cell*. 129:499–510. http://dx.doi.org/10.1016/j.cell.2007.03.027

Krick, R., S. Bremer, E. Welter, P. Schlotterhose, Y. Muehe, E.L. Eskelinen, and M. Thumm. 2010. Cdc48/p97 and Shp1/p47 regulate autophagosome biogenesis in concert with ubiquitin-like Atg8. *J. Cell Biol.* 190:965–973. http://dx.doi.org/10.1083/jcb.201002075

Lampson, M.A., and I.M. Cheeseman. 2011. Sensing centromere tension: Aurora B and the regulation of kinetochore function. *Trends Cell Biol.* 21:133–140. http://dx.doi.org/10.1016/j.tcb.2010.10.007

Le Bot, N., M.C. Tsai, R.K. Andrews, and J. Ahringer. 2003. TAC-1, a regulator of microtubule length in the *C. elegans* embryo. *Curr. Biol.* 13:1499–1505. http://dx.doi.org/10.1016/S0960-9822(03)00577-3

Lee, K., and K. Rhee. 2011. PLK1 phosphorylation of pericentrin initiates centrosome maturation at the onset of mitosis. *J. Cell Biol.* 195:1093–1101. http://dx.doi.org/10.1083/jcb.201106093

Liu, Q., and J.V. Ruderman. 2006. Aurora A, mitotic entry, and spindle bipolarity. *Proc. Natl. Acad. Sci. USA*. 103:5811–5816. http://dx.doi.org/10.1073/pnas.0601425103

Matthews, L.R., P. Carter, D. Thierry-Mieg, and K. Kemphues. 1998. ZYG-9, a *Caenorhabditis elegans* protein required for microtubule organization and function, is a component of meiotic and mitotic spindle poles. *J. Cell Biol.* 141:1159–1168. http://dx.doi.org/10.1083/jcb.141.5.1159

Mchedlishvili, N., S. Wieser, R. Holtackers, J. Mouysset, M. Belwal, A.C. Amaro, and P. Meraldi. 2012. Kinetochores accelerate centrosome separation to ensure faithful chromosome segregation. *J. Cell Sci.* 125:906–918. http://dx.doi.org/10.1242/jcs.091967

McNally, F.J. 2013. Mechanisms of spindle positioning. *J. Cell Biol.* 200:131–140. http://dx.doi.org/10.1083/jcb.201210007

Meyer, H., and O. Popp. 2008. Role(s) of Cdc48/p97 in mitosis. *Biochem. Soc. Trans.* 36:126–130. http://dx.doi.org/10.1042/BST0360126

Meyer, H.H., J.G. Shorter, J. Seemann, D. Pappin, and G. Warren. 2000. A complex of mammalian ufd1 and npl4 links the AAA-ATPase, p97, to ubiquitin and nuclear transport pathways. *EMBO J.* 19:2181–2192. http://dx.doi.org/10.1093/emboj/19.10.2181

Meyer, H., M. Bug, and S. Bremer. 2012. Emerging functions of the VCP/p97 AAA-ATPase in the ubiquitin system. *Nat. Cell Biol.* 14:117–123. http://dx.doi.org/10.1038/ncb2407

Morin, X., and Y. Bellaïche. 2011. Mitotic spindle orientation in asymmetric and symmetric cell divisions during animal development. *Dev. Cell*. 21:102–119. http://dx.doi.org/10.1016/j.devcel.2011.06.012

Mouysset, J., A. Deichsel, S. Moser, C. Hoege, A.A. Hyman, A. Gartner, and T. Hoppe. 2008. Cell cycle progression requires the CDC-48UFD-1/NPL-4 complex for efficient DNA replication. *Proc. Natl. Acad. Sci. USA*. 105:12879–12884. http://dx.doi.org/10.1073/pnas.0805944105

Noatynska, A., C. Panbianco, and M. Gotta. 2010. SPAT-1/Bora acts with Polo-like kinase 1 to regulate PAR polarity and cell cycle progression. *Development*. 137:3315–3325. http://dx.doi.org/10.1242/dev.055293

O'Connell, K.F., K.N. Maxwell, and J.G. White. 2000. The spd-2 gene is required for polarization of the anteroposterior axis and formation of the sperm asters in the *Caenorhabditis elegans* zygote. *Dev. Biol.* 222:55–70. http://dx.doi.org/10.1006/dbio.2000.9714

Persico, A., R.I. Cervigni, M.L. Barretta, D. Corda, and A. Colanzi. 2010. Golgi partitioning controls mitotic entry through Aurora-A kinase. *Mol. Biol. Cell*. 21:3708–3721. http://dx.doi.org/10.1091/mbc.E10-03-0243

Piano, F., A.J. Schetter, M. Mangone, L. Stein, and K.J. Kemphues. 2000. RNAi analysis of genes expressed in the ovary of *Caenorhabditis elegans*. *Curr. Biol.* 10:1619–1622. http://dx.doi.org/10.1016/S0960-9822(00)00869-1

Portier, N., A. Audhya, P.S. Maddox, R.A. Green, A. Dammermann, A. Desai, and K. Oegema. 2007. A microtubule-independent role for centrosomes and Aurora A in nuclear envelope breakdown. *Dev. Cell*. 12:515–529. http://dx.doi.org/10.1016/j.devcel.2007.01.019

Ramadan, K., R. Bruderer, F.M. Spiga, O. Popp, T. Baur, M. Gotta, and H.H. Meyer. 2007. Cdc48/p97 promotes reformation of the nucleus by extracting the kinase Aurora B from chromatin. *Nature*. 450:1258–1262. http://dx.doi.org/10.1038/nature06388

Raman, M., C.G. Havens, J.C. Walter, and J.W. Harper. 2011. A genome-wide screen identifies p97 as an essential regulator of DNA damage-dependent CDT1 destruction. *Mol. Cell*. 44:72–84. http://dx.doi.org/10.1016/j.molcel.2011.06.036

Rape, M., T. Hoppe, I. Gorr, M. Kalocay, H. Richly, and S. Jentsch. 2001. Mobilization of processed, membrane-tethered SPT23 transcription factor by CDC48(UFD1/NPL4), a ubiquitin-selective chaperone. *Cell*. 107:667–677. http://dx.doi.org/10.1016/S0092-8674(01)00595-5

Santaguida, S., C. Vernieri, F. Villa, A. Ciliberto, and A. Musacchio. 2011. Evidence that Aurora B is implicated in spindle checkpoint signalling independently of error correction. *EMBO J.* 30:1508–1519. http://dx.doi.org/10.1038/emboj.2011.70

Sardon, T., I. Peset, B. Petrova, and I. Vernos. 2008. Dissecting the role of Aurora A during spindle assembly. *EMBO J.* 27:2567–2579. http://dx.doi.org/10.1038/emboj.2008.173

Sasagawa, Y., K. Yamanaka, S. Nishikori, and T. Ogura. 2007. *Caenorhabditis elegans* p97/CDC-48 is crucial for progression of meiosis I. *Biochem. Biophys. Res. Commun.* 358:920–924. http://dx.doi.org/10.1016/j.bbrc.2007.05.022

Sasagawa, Y., K. Yamanaka, Y. Saito-Sasagawa, and T. Ogura. 2010. *Caenorhabditis elegans* UBX cofactors for CDC-48/p97 control spermatogenesis. *Genes Cells*. 15:1201–1215. http://dx.doi.org/10.1111/j.1365-2443.2010.01454.x

Sasagawa, Y., A. Higashitani, T. Urano, T. Ogura, and K. Yamanaka. 2012. CDC-48/p97 is required for proper meiotic chromosome segregation via controlling AIR-2/Aurora B kinase localization in *Caenorhabditis elegans*. *J. Struct. Biol.* 179:104–111. http://dx.doi.org/10.1016/j.jsb.2012.06.009

Schuberth, C., and A. Buchberger. 2008. UBX domain proteins: major regulators of the AAA ATPase Cdc48/p97. *Cell. Mol. Life Sci.* 65:2360–2371. http://dx.doi.org/10.1007/s00018-008-8072-8

Schumacher, J.M., N. Ashcroft, P.J. Donovan, and A. Golden. 1998. A highly conserved centrosomal kinase, AIR-1, is required for accurate cell cycle progression and segregation of developmental factors in *Caenorhabditis elegans* embryos. *Development*. 125:4391–4402.

Silkworth, W.T., I.K. Nardi, R. Paul, A. Mogilner, and D. Cimini. 2012. Timing of centrosome separation is important for accurate chromosome segregation. *Mol. Biol. Cell*. 23:401–411. http://dx.doi.org/10.1091/mbc.E11-02-0095

Slep, K.C. 2010. Structural and mechanistic insights into microtubule end-binding proteins. *Curr. Opin. Cell Biol.* 22:88–95. http://dx.doi.org/10.1016/j.ceb.2009.10.009

Song, M.H., L. Aravind, T. Müller-Reichert, and K.F. O'Connell. 2008. The conserved protein SZY-20 opposes the Plk4-related kinase ZYG-1 to limit centrosome size. *Dev. Cell*. 15:901–912. http://dx.doi.org/10.1016/j.devcel.2008.09.018

Spilker, A.C., A. Rabilotta, C. Zbinden, J.C. Labbé, and M. Gotta. 2009. MAP kinase signaling antagonizes PAR-1 function during polarization of the early *Caenorhabditis elegans* embryo. *Genetics*. 183:965–977. http://dx.doi.org/10.1534/genetics.109.106716

Srayko, M., S. Quintin, A. Schwager, and A.A. Hyman. 2003. *Caenorhabditis elegans* TAC-1 and ZYG-9 form a complex that is essential for long astral and spindle microtubules. *Curr. Biol.* 13:1506–1511. http://dx.doi.org/10.1016/S0960-9822(03)00597-9

Srayko, M., A. Kaya, J. Stamford, and A.A. Hyman. 2005. Identification and characterization of factors required for microtubule growth and nucleation in the early *C. elegans* embryo. *Dev. Cell*. 9:223–236. http://dx.doi.org/10.1016/j.devcel.2005.07.003

Steigemann, P., C. Wurzenberger, M.H. Schmitz, M. Held, J. Guizetti, S. Maar, and D.W. Gerlich. 2009. Aurora B-mediated abscission checkpoint protects against tetraploidization. *Cell*. 136:473–484. http://dx.doi.org/10.1016/j.cell.2008.12.020

Strome, S., J. Powers, M. Dunn, K. Reese, C.J. Malone, J. White, G. Seydoux, and W. Saxton. 2001. Spindle dynamics and the role of gamma-tubulin in early *Caenorhabditis elegans* embryos. *Mol. Biol. Cell*. 12:1751–1764.

Thoma, C.R., A. Toso, K.L. Gutbrodt, S.P. Reggi, I.J. Frew, P. Schraml, A. Hergovich, H. Moch, P. Meraldi, and W. Krek. 2009. VHL loss causes spindle misorientation and chromosome instability. *Nat. Cell Biol.* 11:994–1001. http://dx.doi.org/10.1038/ncb1912

Toya, M., Y. Iida, and A. Sugimoto. 2010. Imaging of mitotic spindle dynamics in *Caenorhabditis elegans* embryos. *Methods Cell Biol.* 97:359–372. http://dx.doi.org/10.1016/S0091-679X(10)97019-2

Toya, M., M. Terasawa, K. Nagata, Y. Iida, and A. Sugimoto. 2011. A kinase-independent role for Aurora A in the assembly of mitotic spindle microtubules in *Caenorhabditis elegans* embryos. *Nat. Cell Biol.* 13:708–714. http://dx.doi.org/10.1038/ncb2242

Toyoshima, F., and E. Nishida. 2007. Integrin-mediated adhesion orients the spindle parallel to the substratum in an EB1- and myosin X-dependent manner. *EMBO J.* 26:1487–1498. http://dx.doi.org/10.1038/sj.emboj.7601599

Tsai, M.Y., and Y. Zheng. 2005. Aurora A kinase-coated beads function as microtubule-organizing centers and enhance RanGTP-induced spindle assembly. *Curr. Biol.* 15:2156–2163. http://dx.doi.org/10.1016/j.cub.2005.10.054

Tyson, J.J., and B. Novak. 2008. Temporal organization of the cell cycle. *Curr. Biol.* 18:R759–R768. http://dx.doi.org/10.1016/j.cub.2008.07.001

Uchiyama, K., and H. Kondo. 2005. p97/p47-Mediated biogenesis of Golgi and ER. *J. Biochem.* 137:115–119. http://dx.doi.org/10.1093/jb/mvi028

Uchiyama, K., E. Jokitalo, M. Lindman, M. Jackman, F. Kano, M. Murata, X. Zhang, and H. Kondo. 2003. The localization and phosphorylation of p47 are important for Golgi disassembly-assembly during the cell cycle. *J. Cell Biol.* 161:1067–1079. http://dx.doi.org/10.1083/jcb.200303048

Uchiyama, K., G. Totsukawa, M. Puhka, Y. Kaneko, E. Jokitalo, I. Dreveny, F. Beuron, X. Zhang, P. Freemont, and H. Kondo. 2006. p37 is a p97 adaptor required for Golgi and ER biogenesis in interphase and at the end of mitosis. *Dev. Cell.* 11:803–816. http://dx.doi.org/10.1016/j.devcel.2006.10.016

Wright, A.J., and C.P. Hunter. 2003. Mutations in a beta-tubulin disrupt spindle orientation and microtubule dynamics in the early *Caenorhabditis elegans* embryo. *Mol. Biol. Cell.* 14:4512–4525. http://dx.doi.org/10.1091/mbc.E03-01-0017

Ye, Y. 2006. Diverse functions with a common regulator: ubiquitin takes command of an AAA ATPase. *J. Struct. Biol.* 156:29–40. http://dx.doi.org/10.1016/j.jsb.2006.01.005

Zipperlen, P., A.G. Fraser, R.S. Kamath, M. Martinez-Campos, and J. Ahringer. 2001. Roles for 147 embryonic lethal genes on *C. elegans* chromosome I identified by RNA interference and video microscopy. *EMBO J.* 20:3984–3992. http://dx.doi.org/10.1093/emboj/20.15.3984